

# Compound events in Germany in 2018: drivers and case studies

Elena Xoplaki<sup>1,2</sup>, Florian Ellsäßer<sup>2,a</sup>, Jens Grieger<sup>3</sup>, Katrin M. Nissen<sup>3</sup>, Joaquim G. Pinto<sup>4</sup>, Markus Augenstein<sup>4</sup>, Ting-Chen Chen<sup>4</sup>, Hendrik Feldmann<sup>4</sup>, Petra Friederichs<sup>5</sup>, Daniel Glikzman<sup>6,7</sup>, Laura Goulier<sup>8</sup>, Karsten Hausteiner<sup>9,b</sup>, Jens Heinke<sup>10</sup>, Lisa Jach<sup>11</sup>, Florian Knutzen<sup>9</sup>, Stefan Kollet<sup>8</sup>, Jürg Luterbacher<sup>1,2</sup>, Niklas Luther<sup>2</sup>, Susanna Mohr<sup>4,12</sup>, Christoph Mudersbach<sup>13</sup>, Christoph Müller<sup>10</sup>, Efi Rousi<sup>14</sup>, Felix Simon<sup>13</sup>, Laura Suarez-Gutierrez<sup>15,c,d</sup>, Svenja Szemkus<sup>5</sup>, Sara M. Vallejo-Bernal<sup>16,17</sup>, Odysseas Vlachopoulos<sup>2</sup>, Frederik Wolf<sup>16</sup>

<sup>1</sup> Department of Geography, Climatology, Climate Dynamics and Climate Change, Justus Liebig University Giessen, Giessen, Germany

<sup>2</sup> Centre of International Development and Environmental Research, Justus Liebig University Giessen, Giessen, Germany

<sup>3</sup> Institute of Meteorology, Free University of Berlin, Berlin, Germany

<sup>4</sup> Institute of Meteorology and Climate Research (IMK-TRO), Karlsruhe Institute of Technology (KIT), Karlsruhe, Germany

<sup>5</sup> Institute of Geosciences, University of Bonn, Bonn, Germany

<sup>6</sup> Institute of Hydrology and Meteorology, Faculty of Environmental Sciences, Dresden University of Technology, Tharandt, Germany

<sup>7</sup> Institute of Geography, Dresden University of Technology, Dresden, Germany

<sup>8</sup> Institute for Bio- and Geosciences, Research Centre Jülich, Jülich, Germany

<sup>9</sup> Climate Service Center Germany (GERICS), Helmholtz-Zentrum Hereon, Hamburg, Germany

<sup>10</sup> Potsdam Institute for Climate Impact Research (PIK), Member of the Leibniz Association, Potsdam, Germany

<sup>11</sup> Institute of Physics and Meteorology, University of Hohenheim, Stuttgart, Germany

<sup>12</sup> Center for Disaster Management and Risk Reduction Technology (CEDIM), Karlsruhe Institute of Technology, Karlsruhe, Germany

<sup>13</sup> Department of Hydraulic Engineering and Hydromechanics, Civil and Environmental Engineering, Bochum University of Applied Sciences, Bochum, Germany

<sup>14</sup> Potsdam Institute for Climate Impact Research (PIK), Member of the Leibniz Association, Potsdam, Germany

<sup>15</sup> Max-Planck-Institut für Meteorologie, Hamburg, Germany

<sup>16</sup> Research Department IV - Complexity Science, Potsdam Institute for Climate Impact Research (PIK), Member of the Leibniz Association, Potsdam, Germany

<sup>17</sup> Institute of Geosciences, University of Potsdam, Potsdam, Germany

<sup>a</sup> now at: Department of Natural Resources, ITC - Faculty of Geoinformation Science and Earth Observation, University of Twente, The Netherlands

<sup>b</sup> now at: Institute for Meteorology, University of Leipzig, Leipzig, Germany

<sup>c</sup> now at: Institute for Atmospheric and Climate Science, ETH Zurich, Zurich, Switzerland

<sup>d</sup> now at: Institut Pierre-Simon Laplace, CNRS, Paris, France

*Correspondence to:* Elena Xoplaki (elena.xoplaki@geogr.uni-giessen.de)

**Abstract.** Europe frequently experiences a wide range of extreme events and natural hazards, including heatwaves, extreme precipitation, droughts, cold spells, windstorms, and storm surges. Many of these events do not occur as single extreme events, but rather show a multivariate character, known as compound events. We investigate the interactions between extreme weather events, their characteristics, changes in intensity, frequency, as well as uncertainties in the past, present and future. We also explore their impacts on various socio-economic sectors in Germany and Central Europe. This contribution highlights several case studies with special focus on 2018, a year marked by an exceptional sequence of compound events across large parts of Europe, resulting in severe impacts on human lives, ecosystems, and infrastructure. We provide new insights into the drivers of spatially and temporally compound events, such as heat and drought and heavy precipitation combined with extreme winds, and their adverse effects on ecosystems and society, using large-scale atmospheric patterns. We also examine the interannual influence of droughts on surface water, and the impact of water scarcity and heatwaves on agriculture and forests. We assess projected changes in compound events at different current and future global surface temperature levels, demonstrating the need for improved quantification of future extreme events to support adaptation planning. Finally, we address research gaps and future directions, stressing the importance of defining composite events primarily in terms of their impacts prior to their statistical characterisation.

## 51 **1 Introduction**

52 Extreme temperatures, strong extratropical low pressure systems and their associated extreme winds and heavy precipitation  
53 events can have devastating socio-economic impacts. Moreover, the combination of otherwise regular climate and weather  
54 phenomena can unfold their effects beyond the individual events (Ridder et al., 2020) and have devastating consequences and  
55 impacts (Ridder et al., 2022; Bevacqua et. al., 2017, 2021, 2023 and references therein). Thus, human and natural systems that  
56 are usually able to handle the impacts of single extreme events are challenged by the co-occurrence of two or more extremes  
57 (compound events, CE) which severely increase the risk of loss and damage (Toreti et al., 2019a). Events with additive and  
58 multiplicative effects are of utmost importance and can result from mutually reinforcing cycles/positive feedback between  
59 individual events. Interrelated events, e.g., through land surface-atmosphere interactions or atmospheric moisture conditions,  
60 modify extreme events (Wang et al., 2022). The effects may develop also through atmospheric dynamics that connect features  
61 such as the 2010 Russian heatwave and the flood in Pakistan (Barriopedro et al., 2011; Lau et al., 2012; Zscheischler et al.,  
62 2018) or through induced responses at distant areas of significant impact to the global system (Vogel et al., 2019).

63 The Intergovernmental Panel on Climate Change (IPCC; Seneviratne et al., 2012) defines CEs as 1) two or more extreme  
64 events occurring simultaneously or successively, 2) a combination of extreme events with underlying conditions that amplify  
65 the impact of the events, or 3) a combination of events that are not themselves extremes but lead to an extreme event or impact  
66 when combined. This definition is embedded within the IPCC risk framework under the umbrella of a combination of multiple  
67 drivers and/or hazards that contribute to societal or environmental risks. Also embedded in this framework is the understanding  
68 that response to an imminent risk can, in its own right, serve to reduce or to increase future risks. CEs often lead to  
69 disproportionate impacts on people and ecosystems (Seneviratne et al., 2012; Leonard et al., 2014; Caldeira et al., 2015; Bastos  
70 et al., 2021). To quantify the probability of CEs in today's and future climate is of great importance specifically for adaptation  
71 planning for various sectors including agriculture, fisheries, river transport, energy supply, tourism, etc. (Zscheischler and  
72 Fischer, 2020). Recently, Zscheischler et al. (2020) extended the definition and classified CEs into 1) preconditioned events,  
73 where a weather-driven or climate-driven precondition aggravates the impacts of a climatic impact-driver; 2) multivariate  
74 events, where multiple drivers and/or climatic impact-drivers lead to an impact; 3) temporally compounding events, where a  
75 succession of hazards leads to an impact; and 4) spatially compounding events, where hazards in multiple connected locations  
76 cause an aggregated impact. Drivers include processes, variables, and phenomena in the climate and weather domain that may  
77 span over multiple spatial and temporal scales (Zscheischler et al., 2020). Current research on weather and climate impacts,  
78 risks and damages often underestimates the influence of CEs (Ridder et al., 2021). It is therefore essential to adapt research  
79 strategies and tools, such as models, to integrate compound weather and climate events, enabling a more accurate assessment  
80 of uncertainties, impacts and risks. Further, anthropogenic climate change is expected to influence the frequency and intensity  
81 of CEs, and thus future planning for such changes requires reliable climate models, which can represent these hazards, their  
82 underlying drivers as well as their combinations. Despite this importance, studies evaluating climate model representation of  
83 CEs are still rare (Aalbers et al., 2013; Bevacqua et al., 2023; Manning et al., 2023). Further, the impact of climate change to  
84 dynamic changes in the atmosphere and consequently to the location and magnitude of extreme events and its compounds is  
85 less well understood and thus characterised as low confidence by the IPCC (IPCC, 2021). This holds true also for CEs, which  
86 are naturally even more complex due to their multivariate character, also in terms of the complexity of the atmospheric  
87 circulation state. For instance, the COVID-19 pandemic has brought dynamics of compound hazards and risk-response  
88 feedback to the forefront of hydrometeorological hazard response and preparedness (Simpson et al., 2021; Zaitchik et al.,  
89 2022). Compound hazards are rare, and those for instance that involve a disease such as COVID-19 have no recent precedent.

90 The more complex CEs become, the clearer are the limitations of the conventional statistical approaches to risk assessment  
91 (Zaichik et al., 2022).

92 The development of integrated research on CEs is the objective of the European COST Action DAMOCLES  
93 (<http://www.damocles.compoudevents.org>) that bundled research efforts in this field, and towards which several of the  
94 authors actively contribute. One of the main knowledge gaps identified concerns how the compound character of events is  
95 changing in a warming world and will continue to change during future decades. The question on how and why extreme  
96 weather events affecting specifically Germany and Central Europe may change in a warming climate is the major topic of the  
97 climXtreme project (<https://climxtreme.net/>), in the frame of which this work has been conducted, aiming to analyze and  
98 understand the dynamics of extreme climate events, their impacts, and potential future trends in a changing climate. To analyse  
99 hot and dry compounds, a variety of research questions and approaches are explored: at the global scale, the precursors of  
100 spatially and temporally CEs are analysed using large-scale atmospheric patterns and jet stream states. At the European scale,  
101 the detection and identification of events and the spatial representation of key climate variables in relation to heatwaves are  
102 investigated. Focusing on Germany, the interannual influence of droughts on surface water is analysed and the impact of water  
103 scarcity and heatwaves on agriculture and forests is studied. Further, the CEs including precipitation and/or wind as a hazard  
104 are analysed focusing on a series of windstorms and convective storms with adverse impacts on ecosystems and society.

105 All case studies presented in this paper are selected from the calendar year 2018, which is of particular interest given the  
106 prolonged and persistent dry and hot conditions across large parts of Europe as well as featured storms Eleanor and David  
107 (coined Burglind and Friederike in Germany and hereafter) in January 2018 and several weeks of thunderstorm activity in May  
108 and June. 2018 was also characterized by strong wind gusts that co-occurred with heavy snowfall during the windstorm  
109 Friederike (Vautard et al., 2019), a relatively dry spring with exceptionally high temperatures followed by an extremely dry  
110 summer with very warm mean temperatures over large areas of Europe (Munich Re, 2019; Zscheischler and Fischer, 2020).  
111 Total precipitation in central Europe was at the lowest percentiles relative to the 1976–2005 distribution; Germany experienced  
112 a reduction of precipitation of ~53% in July and of ~46% in August compared to the period 1981–2010 (Deutscher  
113 Wetterdienst, 2018). The summer in Germany was characterised by the most extreme combination of high temperatures, as  
114 one of the warmest years on record (Kaspar et al., 2023) and low precipitation since 1881 (Zscheischler and Fischer, 2020).  
115 The combination of the individual events caused tremendous adverse and detrimental impacts in larger areas of western Europe  
116 with a peak over Germany and on a variety of sectors ranging from agriculture and society (Manning et al., 2018; Toreti et al.,  
117 2019b; Zscheischler and Fischer, 2020; Conradt et al., 2023; Shyrokaya et al., 2024), forests (Bastos et al., 2020; Buras et al.,  
118 2020; de Brito et al., 2020; Senf and Seidl, 2021), fires (Munich Re 2019; Bastos et al., 2020), ecology (Bastos et al., 2021),  
119 soil and surface water (Liu et al., 2020; Brakkee et al., 2022; Hartick et al., 2021), marine environment (Kaiser et al., 2023),  
120 traffic disruption, power outages, property damage by e.g. falling trees, fatalities (Vautard et al., 2019) as well as human health  
121 (Matzarakis et al., 2020; Conradt et al., 2023). The exceptional heatwave of 2018 also caused many nuclear power plants to  
122 shut down because the rivers could not provide sufficient cooling capacity for the reactors (Vogel et al., 2019). In addition,  
123 Blauhut et al. (2022) surveyed stakeholders across Europe regarding their perceptions of the 2018–2019 drought and drought  
124 risk management in their respective countries. Germany was identified as being aware of drought risks but among the least  
125 prepared, lacking a formal management plan.

126 We study this exceptional year and the series of extremes and CEs in a sequence of the large scale, their detection and spatial  
127 representation as well as the long term impacts on soil moisture both at the continental scale and the consequent agriculture  
128 and forestry impacts at the national scale. The paper first outlines the data and methodologies used for analysing the selected  
129 CEs in 2018, followed by a detailed analysis of each case study. These case studies are categorized into temperature-  
130 precipitation and precipitation-wind CE storylines, along with an evaluation of their impacts in Germany.

## 131 **2 Data and Methods**

132 Different methodological approaches have been used, tailored to the different types of CEs, ranging from better understanding  
133 of the selected event drivers to sectoral impact assessments. This section summarizes these approaches and provides a basis  
134 for the study and analysis of the selected case studies separated in temperature-precipitation and precipitation-wind CEs. The  
135 temperature-precipitation storyline includes analysis on drivers of the hot summer of 2018, detection of extreme events and  
136 spatial patterns, assessment of the impact of the 2018 European drought on soil moisture and groundwater as well as sectoral  
137 impacts on agriculture and forestry. The storyline is complemented with an assessment of model simulations to realistically  
138 represent conditions as those of 2018 in Germany. The precipitation-wind storyline comprises the analysis of intense low  
139 pressure systems in winter 2018, their life cycle and triggering role for compound precipitation and wind events, as well as  
140 severe convective storms during the 2018 warm season. Considering the nature of the various case studies and events during  
141 the warm season of 2018, and given the focus on compound events in this study, we aim to define the characteristics of the  
142 events analysed and their interrelationships. Additionally, a range of relative thresholds, such as the 90th, 95th, and 98th  
143 percentiles, appropriate for each variable and elaborated impact are used to define extremes, and we will provide explanations  
144 for their application.  
145

### 146 **2.1 Drivers of the hot summer of 2018**

147 To better understand the drivers of the hot summer of 2018, Rousi et al. (2022) identified jet states in the zonal mean zonal  
148 wind over the Eurasian sector at different pressure levels for the summer months in ERA5 data (Hersbach et al., 2020) using  
149 Self-Organizing Maps (SOMs, see Kohonen, 2013; Rousi et al., 2015). A comparative approach with different cluster numbers,  
150 clustering algorithms and initializations of SOMs led to a robust cluster of double jet states. Increased persistence of those jet  
151 states was connected to heatwave events (defined as a period of at least 3 consecutive days of daily maximum temperature  
152 threshold exceedance > 90th percentile, following Fischer and Schär (2010) and a spatial extent over 40.000 km<sup>2</sup> within a 4°  
153 x 4° spatial sliding window, similar to Stefanon et al. (2012) across western Europe (Rousi et al., 2022).

### 154 **2.2 Detection of spatial patterns of extreme events**

155 The analysis of the large-scale temperature and precipitation deficit patterns and their expression during the 2018 heatwave at  
156 the European scale is based on the cross-Tail Pairwise Dependence Matrix (cross-TPDM) and Extreme Pattern Index (EPI)  
157 proposed by Szemkus and Friederichs (2024). Typical spatial patterns of common extremes are derived by singular value  
158 decomposition of the cross-TPDM. The cross-TPDM is a measurement of extremal dependence, rooted in extreme value theory  
159 and has comparable statistical properties to the cross-covariance matrix (Szemkus and Friederichs, 2024; Cooley and Thibaud,  
160 2019). The singular vectors of cross-TPDM represent pairs of spatial patterns in which extremes in two variables are likely to  
161 occur simultaneously. Consequently, the expansion coefficients provide a time series for each singular vector that summarise  
162 the occurrence of extreme events within the respective pattern. The first 10 left and right expansion coefficients are then  
163 summarised in the EPI that is high when individual patterns or a linear combination of leading patterns are particularly strongly  
164 pronounced. This pattern-based analysis thus provides a robust measurement for the heatwave and drought intensity over  
165 Europe. Before calculating the cross-TPDM and EPI, the ERA5 daily 2m temperature and precipitation deficits for the summer  
166 months (June–August) of 2018 are standardised and the annual cycle is removed. Precipitation deficits are calculated as the  
167 inverse of the 90-day accumulated precipitation.

### 168 **2.3 Surface water storage of the dry summer of 2018**

169 To analyse the drought characteristics of the summer of 2018, an ensemble of simulations for the hydrological year 2018/19  
170 is used (Hartick et al., 2021). The hydrological year 2018/2019 was initialised with land surface and subsurface conditions

171 from the end of the hydrological year 2018 and simulated using different atmospheric boundary conditions. The proposed  
172 approach investigates the impact of hydrologic initialization, and soil and groundwater memory on water storage anomalies  
173 against the background of atmospheric variability and uncertainty on an interannual time scale. The varying atmospheric initial  
174 conditions were derived from the ERA-Interim data for each individual year between 1996 and 2018 and resulted in 22  
175 realisations as the number of individual years within that period. Thus, the ensemble of realisations of the hydrological year  
176 2018/2019 accounts for a large part of the atmospheric uncertainty. The analysis was performed for 20 European river basins.  
177 The 2018 drought was defined as the driest 10% of the total water storage anomalies (S) occurring in 2018 within the  
178 climatological time series. Surface water availability for the 2018/2019 hydrological year was represented by surface water  
179 storage ( $S_u$ ), categorised into dry,  $S_{u,d}$ , and wet,  $S_{u,w}$ , anomalies. To ensure that an increased probability of  $S_{u,d}$  in the  
180 hydrological year 2018/2019 was outside of regular climate variability, we compared the  $S_{u,d}$  probability distribution of the  
181 described hydrological year 2018/2019 ensemble (Case a) with the probability distribution of  $S_{u,d}$  within the climatological  
182 time series (Case b), see also the corresponding section below. Two beta distributions were generated, one for each case, by  
183 applying a prior with no information. We sampled each beta distribution 10,000 times and calculated the probability of Case  
184 a > Case b to determine the confidence that the probability of a  $S_{u,d}$  after a drought is greater than the climatological variability.  
185 In addition, we obtained the uncertainty of the confidence intervals by bootstrapping 1000 times over the climatological time  
186 series. The methodology provides a probabilistic insight into the impact of a groundwater drought on future surface water  
187 resources on an interannual time scale.

#### 188 **2.4 Soil moisture of the dry summer of 2018**

189 In addition to the dry surface water anomaly in Central Europe, soils showed moisture deficits (Liu et al., 2020; Bastos et al.,  
190 2020; Rousi et al., 2023; Conradt et al., 2023). This likely caused low groundwater levels (Brauns et al., 2020; Conradt et al.,  
191 2023), as infiltration of precipitation water is considered to be the most important groundwater source in Central Europe  
192 (Brakkee et al., 2022). ERA5 soil moisture was evaluated for the four soil layers over the period 2018-2020 and compared  
193 against the climatology averaged over 1991-2020 in order to assess the strength of the soil moisture deficit and its persistence  
194 during the consecutive drought years 2018-2020. For this analysis, time series of daily means as well as centred 92-day running  
195 means were computed for all land points of the study area 4°-16° E and 45°-55° N, covering Germany and adjacent regions.  
196 The evaluation of soil moisture in the lowest soil layer also gives an indication of the groundwater reservoir as it interacts with  
197 the aquifer in the modelling system (Cerlini et al., 2021).

#### 198 **2.5 Agricultural and hydrological drought of the year 2018**

199 Lack of sufficient soil moisture, resulting from shortage of precipitation and excess evapotranspiration leads to agricultural  
200 drought. Lack of run-off and surface water result in hydrological drought (streamflow deficits) (Seneviratne et al., 2021). To  
201 estimate the severity of agricultural and hydrological droughts across Europe during summer 2018, we employed the nitrogen  
202 version of the vegetation, crop, and hydrology model LPJmL (Schaphoff, et al., 2018; von Bloh et al., 2018; Lutz et al., 2019;  
203 Herzfeld et al., 2021). The analysis is based on 69 years (1951-2019) obtained from model simulations driven with daily  
204 temperature, precipitation, and radiation data from the GSWP-W5E5 dataset (Kim, 2017; Cucchi et al., 2020; Lange et al.,  
205 2022) at 0.5 arc-degree resolution. To assess agricultural drought, the evapotranspiration deficit calculated as the ratio of actual  
206 evapotranspiration to potential evapotranspiration (ET/PET ratio) over the growing season of maize in each year is determined  
207 and a generalised beta distribution (a three-parameter probability distribution for variables in a bounded interval) is fitted to  
208 the 69 annual values in each grid cell. An ET/PET ratio of less than 1 indicates water deficit or water stress. For the assessment  
209 of the hydrological drought, the average river discharge (Dis) during the summer months (June, July, and August) of each year  
210 is determined and a generalized gamma distribution (a three-parameter probability distribution for non-negative variables) is  
211 fitted to the 69 annual values in each grid cell. Using the fitted distributions, the return period of the conditions in 2018 is

212 determined. To support comparability with other drought indices such as the Standardized Precipitation Evapotranspiration  
213 Index (SPEI), the drought severity is also calculated, which is the probability (inverse of return period) of a given year  
214 expressed as its distance from the mean (in number of standard deviations) in a standard normal distribution (McKee et al.,  
215 1993; Vicente-Serrano et al., 2010). For example, a return period of 44 years is equivalent to the 2.28th percentile, which is  
216 -2 standard deviations away from the mean and would be assigned a drought severity of -2.

## 217 **2.6 Impact on the agricultural production of 2018**

218 In comparison with the past three decades, the year 2018 was identified as a year with severe winter wheat yield losses  
219 estimated using a compilation of LOESS (locally estimated scatterplot smoothing; to take into account improvement of  
220 agricultural practises (Zampieri et al., 2017)) detrended and gap-filled yield data at county level aggregated from a variety of  
221 sources including the Regionaldatenbank Deutschland (Statistische Ämter des Bundes und der Länder, 2021) and the Statistical  
222 Offices of the federal states of Germany (datasets at JLUpub research data repository: Ellsäßer and Xoplaki 2022abc). The  
223 resulting annual gridded yield data was evaluated using the Standardized Yield Anomaly Index (SYAI) that expresses yield  
224 anomalies in terms of standard deviation from a 30-year time series. The analysis is based on the Heat Magnitude Index (HMD)  
225 (Zampieri et al., 2017), the drought index SPEI (Vicente-Serrano et al., 2010) and the Combined Stress Index (CSI) (Zampieri  
226 et al., 2017) that accounts for stress compounds of heat and drought through a (ride-regression based) superimposition of HMD  
227 and SPEI, using the temperature and precipitation series from E-OBS (Cornes et al., 2018). In order to derive crop relevant  
228 results, all indices were evaluated for the most vulnerable stages of phenological crop development according to the specific  
229 region using the German Weather Service (DWD) phenological data set (Kaspar et al., 2015). A spatially explicit linear  
230 regression between yield anomaly and stress indices was computed for time series covering the past three decades and the  
231 coefficient of determination ( $R^2$ ) was calculated to express the proportion of yield anomaly that can be explained by heat,  
232 drought or compound stress.

## 233 **2.7 Loss and damage of compound vs. non-compound wind extreme events of the winter 2018**

234 The precipitation-wind storyline starts with a description of the synoptic situation during the winter season 2018. The cyclone  
235 track analysis in this section is based on the cyclone tracking methodology of Murray and Simmonds (1991) and Pinto et al.  
236 (2005) applied to ERA5 data (Hersbach et al., 2020).

237 Loss and damage in this section is defined according to the UN Framework Convention on Climate Change (UNFCCC) as the  
238 harm caused by anthropogenic (human-generated) climate change (UNFCCC, 2021; OECD, 2021 and references therein). For  
239 the quantitative assessment of the impact of CEs in terms of loss and damage, a compound wind and precipitation extreme is  
240 defined when both variables exceed their local 98th percentile (Martius et al., 2016). For winter events, these percentiles are  
241 calculated using data from the December to February season. Co-occurrence is defined when wind gusts and precipitation both  
242 exceed their respective 98th percentile at a specific grid box, with precipitation exceedance occurring on the same day, the day  
243 before, or the day after, within a 50 km radius around the grid box centre.

244 The daily loss data for residential buildings accumulated over Germany provided by the German Insurance Association (GDV)  
245 are categorised by days on which a CE occurred and days on which it did not. This results in two separate loss distributions  
246 for compound and non-compound events.

## 248 **2.8 Concurrent heavy rain and storm extremes – estimation of probability of event occurrence**

249 The estimation of the probability of occurrence of compound heavy rain and wind is carried out on precipitation and wind time  
250 series from DWD weather stations. Multivariate distributions in the form of copulas are used to determine the probability of  
251 occurrence of combined events. Copulas make it possible to model the dependency structure of the variables under

252 consideration independently of their marginal distributions (e.g. Manning et al., 2024 and references therein). This allows for  
253 the use of any distribution function for the marginal distributions.

254 We carried out fitting tests for both the marginal distributions and the copulas. However, Archimedean copulas are generally  
255 preferred when dealing with hydrological parameters (Bender, 2015; Jane et al., 2020). In this particular case, the Frank copula  
256 (Frank, 1979) was chosen as the most appropriate option. The Frank copula is a one-parametric copula in which the copula  
257 parameter *theta* can be determined from the correlation between random variables. The approach treats the extremes of the  
258 two variables (rain and wind) separately. The annual maximum values (AMAX) are extracted from the time series and tested  
259 for statistically significant trends using the Mann-Kendall test at a 5% significance level. Stationary methods of extreme value  
260 statistics are applied, requiring the assumption of independence and identical distribution of all time series. Consequently,  
261 series with significant trends are homogenised using linear regression. The distribution parameters of the strong wind and  
262 precipitation data sets are then determined using maximum likelihood. In addition, the correlation between heavy rain and  
263 storm is calculated using the Kendall rank correlation. For each AMAX wind value, the concurrent precipitation value is  
264 selected and vice versa. To ensure the independence of precipitation events, wet episodes are separated by a dry period of at  
265 least as long as the accumulation period. Due to this restriction, not all AMAX wind events can be paired with a precipitation  
266 episode, even when precipitation is present, e.g., for longer precipitation durations (>1 day) and considering a  $\pm 2$ -day window,  
267 no AMAX wind and precipitation episode pairs exist. Subsequently, these pairs of values are applied to adjust the marginal  
268 distributions and copulas, thereby determining the combined probabilities of occurrence.

## 269 **2.9 Rockfall events**

270 Rockfall is an impact that can be triggered by extreme precipitation (e.g., Nissen et al., 2022). Favourable preconditions, such  
271 as previous freeze-thaw cycles and enhanced sub-surface moisture, increase the susceptibility for such events. A logistic  
272 regression model, describing the probability of rockfall in the Central European low mountain ranges as a function of  
273 meteorological (pre-) conditions, was fitted using the Rupp and Damm (2020) database of rockfall events. To find the optimal  
274 statistical model, a large number of models including different atmospheric predictors and interaction terms between the  
275 predictors were compared. The best model was selected based on the logarithmic skill score determined during cross validation.  
276 The best-performing model includes across-site percentile of a fissure water proxy D (precipitation minus potential evaporation  
277 determined for the last 5 days), the local percentile of daily precipitation and the binary information if a freeze-thaw cycle has  
278 occurred within the last 9 days. It also considers the interaction between daily precipitation and D. By including several  
279 meteorological parameters the statistical model describes the multivariate compounding nature of rockfall initialization. By  
280 taking preconditions into account the preconditioned compounding component is addressed. Using the statistical model, a  
281 probability for a rockfall event can be determined for each day from the meteorological conditions of the previous 9 days and  
282 the day itself. Details of the statistical model can be found in Nissen et al. (2022).

## 283 **2.10 Convective cluster events of the summer 2018**

284 Convective cluster events (CCEs) are spatially connected areas of intense lightning activity that occur simultaneously in the  
285 same geographic region. CCEs can be detected using the Spatial-Temporal Density-Based Spatial Clustering of Applications  
286 with Noise (ST-DBSCAN) algorithm (Ester et al., 1996; Birant and Kut, 2007). The data used are cloud-to-ground lightning  
287 strokes from the European Cooperation for Lightning Detection (EUCLID) network (Schultz et al., 2016). ST-DBSCAN is  
288 further developed and specifically adapted for the detection of spatio-temporal clustering of lightning strokes (Augenstein et  
289 al., 2023). The algorithm identifies arbitrarily shaped clusters in a set of given points, which in this case are spatio-temporally  
290 close lightning strokes. For the identification of CCEs, thresholds from sensitivity studies have been used, i.e., if at least 40  
291 lightning strokes occur within 20 minutes and 50 km, single lightning strikes are marked belonging to a CCE. These thresholds  
292 have proven to be an “optimal” balance to distinguish between lightning clusters and noise.

## 293 **2.11 Occurrence of extreme compound events from recent to near-term future climate conditions**

294 The estimation of the projected changes in the frequency of CEs from recent to near-term future climate conditions is based  
295 on the 30-member CMIP6 MPI-GE (Olonscheck et al., 2023). The historical and SSP5-8.5 (Riahi et al., 2017) simulations for  
296 the periods 1975-2025 and 2025-2075 are used, representing climate conditions that for the CMIP6 MPI-GE range from about  
297 1 to 3 °C increase in global mean surface temperature since pre-industrial times (Olonscheck et al., 2023). The projections  
298 cover Germany and more specifically the region defined by the 4°-16° E and 45°-55° N latitude-longitude domain. The  
299 compound heat and drought years are defined by the cumulative precipitation from May to October and the mean daily  
300 maximum temperature from June to August, spatially averaged over Germany. Extreme compound hot and dry years exceed  
301 the 20-year return levels for both precipitation deficit and maximum temperature individually, defined as the 5th and 95th  
302 percentiles, respectively, for the period 1975-2025. The compound precipitation-wind years are defined on the winter  
303 (December to February) daily mean precipitation and daily maximum surface wind. The selection of events is based on the  
304 exceedance of the 98th percentile for wind and precipitation during the period from 1975 to 2025. For each grid cell, wind and  
305 precipitation events are identified when they exceed this threshold on the same day, while for precipitation alone, the  
306 exceedance can occur either on the same day or the day after. The cumulative effect for the whole season is the sum of all  
307 daily occurrences over all winter days and each grid cell. Extreme compound wind and precipitation years exceed the 20-year  
308 return levels for precipitation and wind individually, defined as the 95th percentile of each variable for the period 1975-2025.

## 309 **2.12 Representation of moisture availability of 2018 in model simulations**

310 The performance of model simulations in realistically representing drought conditions like those of 2018 and the 2018-2020  
311 three-year drought cluster of events is assessed based on the estimated trend of the warm season (March to August) moisture  
312 availability in Germany. Drought conditions are described with the SPEI index (Vicente-Serrano et al., 2010) for observations,  
313 using ERA5 data (Hersbach et al., 2020) for the period 1979-2019, and for bilinearly interpolated (regular 0.5° lon-lat grid)  
314 and extended to 2021 ensemble simulations of CMIP5 (Taylor et al., 2012; Aalbers et al., 2023) global circulation models and  
315 of EURO-CORDEX 0.11° (Giorgi et al., 2009) regional multi-model ensemble for the historical (1950-2005) and the near-to-  
316 mid-term future (2006-2070) periods under RCP8.5. The linear trend of the 3-year running mean for the March to August  
317 intervals is calculated over the periods 1975-2021 for the simulations (1979-2019 for ERA5) and 2022-2070 in order to account  
318 for the transition from dimming to brightening regime in the 1970s (Wild, 2009, 2016).

## 319 **3 Compound events in the year 2018**

### 320 **3.1 Temperature-precipitation compound events during 2018**

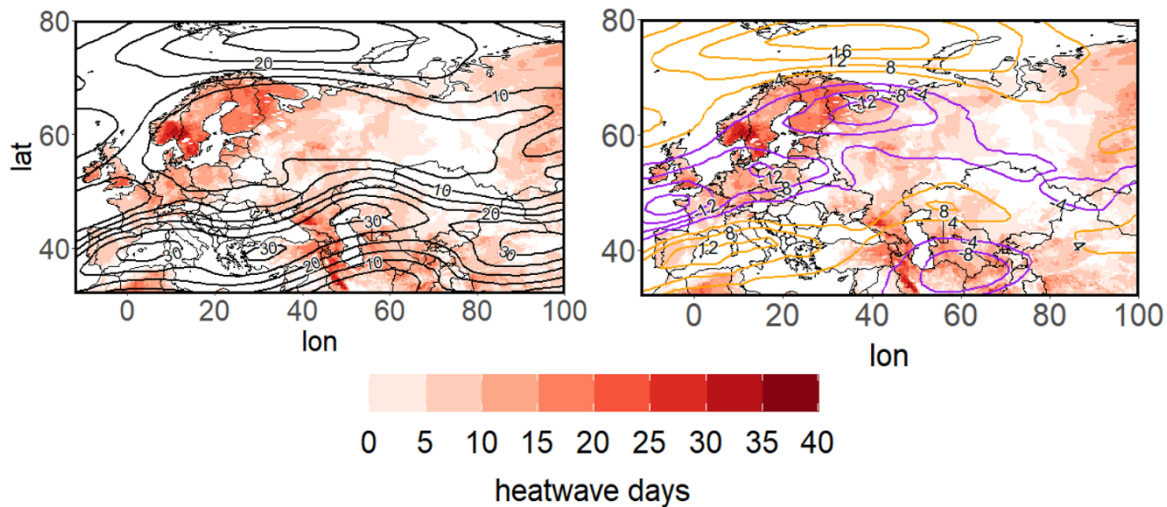
321 The exceptionally hot and dry conditions in 2018 extended over larger areas including central and northern Europe and were  
322 associated with impacts on various economic sectors (e.g. Toreti et al., 2019a; Zscheischler and Fischer, 2020; Bastos et al.,  
323 2023; Conradt et al., 2023; Shyrokaya et al., 2024).

#### 324 **3.1.1 Drivers of the hot summer of 2018**

325 The 2018 heatwave was a spatially CE featuring concurrent heatwaves in Scandinavia and central Europe (Spensberger et al.,  
326 2020; Rousi et al., 2023). Prior to the 2018 heatwave, a striped high-pressure system formed over northern Europe in late June,  
327 during a combination of the positive phase of the North Atlantic Oscillation and the Rossby Wave 7 pattern (Drouard et al.,  
328 2019; Kornhuber et al., 2019). Figure 1 presents the jet stream state during the 2018 summer and the heatwave day frequency  
329 for each grid point over the Eurasian sector. During the intense European summer heatwave, a large blocking system at 500  
330 hPa, and a double jet stream configuration is visible in the 250 hPa zonal wind field (Kornhuber et al., 2019; 2020; Rousi et  
331 al., 2023, see Methods section 2.1). Heatwave hot spots over Europe coincide with areas of weak winds between the polar and



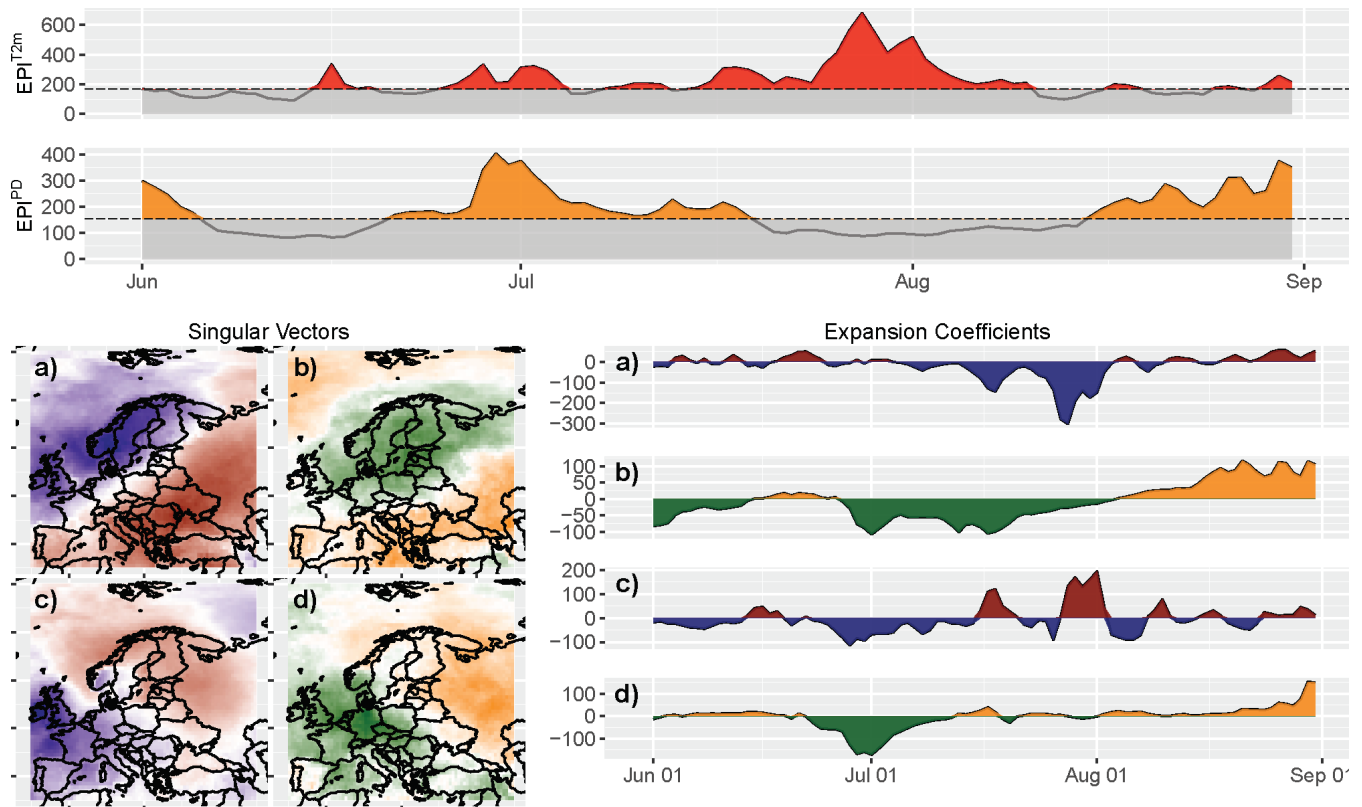
332 subtropical jets. Such large-scale atmospheric conditions are conducive to the occurrence of extreme events over Europe, in  
 333 particular to heatwaves near the centre of the blocking system (see Kautz et al., 2022 for a review). In particular, the hot  
 334 summer of 2003 (western/central Europe, Luterbacher et al., 2004; Fink et al., 2004; Fischer et al., 2007; García-Herrera et al.,  
 335 2010) and 2010 (heatwave over western Russia, Barriopedro et al., 2011; Di Capua et al., 2021; Rousi et al., 2022) were  
 336 characterised by similar large-scale conditions.



337  
 338 **Figure 1: Jet stream state (contour lines) and heatwave days in summer 2018 (shading). Left: zonal wind at 250 hPa (black contours**  
 339 **from 5 m/s to 30 m/s every 5 m/s); Right: zonal wind anomalies at 250 hPa (anomalies based on 1979-2020 July climatology and**  
 340 **plotted with contours from -16 m/s to 16 m/s every 4 m/s, negative anomalies are shown in purple contours and positive in orange)**  
 341 **for the period 4-25 July 2018, the longest period of consecutive double jet states. All fields stem from ERA5 reanalysis data (Hersbach**  
 342 **et al., 2020).**

343  
 344 **3.1.2 Detection of spatial patterns of extreme events**

345 During the summer 2018, large-scale temperature ( $T_{2m}$ ) and precipitation deficit (PD) patterns characterize the exceptional  
 346 conditions. Figure 2 shows the analysis of typical pattern of common extremes and their expression during the 2018 heatwaves  
 347 at the European scale based on cross-TPDM and EPI (see Methods section 2.2). In July-August 2018 the pronounced heatwave  
 348 is accompanied by extreme  $EPI^{PD}$  preceding the heatwave for several days. This heatwave is considered the most prominent  
 349 event in the period under consideration (see also Liu et al., 2020). The negative eigenvector anomalies of the second mode  
 350 (Fig. 2a,b bottom left) mostly cover the regions identified as heatwave spots in Figure 1. Thus, the anomalies in the second  
 351 mode expansion coefficients (Fig. 2a,b bottom right) indicate the beginning of the heatwave, which initially affected northern  
 352 Europe (i.e., Finland, Norway, and northwestern Russia). From mid of June onwards, there were extremes in PD, particularly  
 353 in Central Europe, as indicated by the third mode of the expansion coefficient (Fig. 2c,d bottom right). By the end of July  
 354 2018, the heatwave extended to Central Europe as evidenced from the abrupt change of sign in the third mode expansion  
 355 coefficient (Fig. 2c,d bottom right).



356

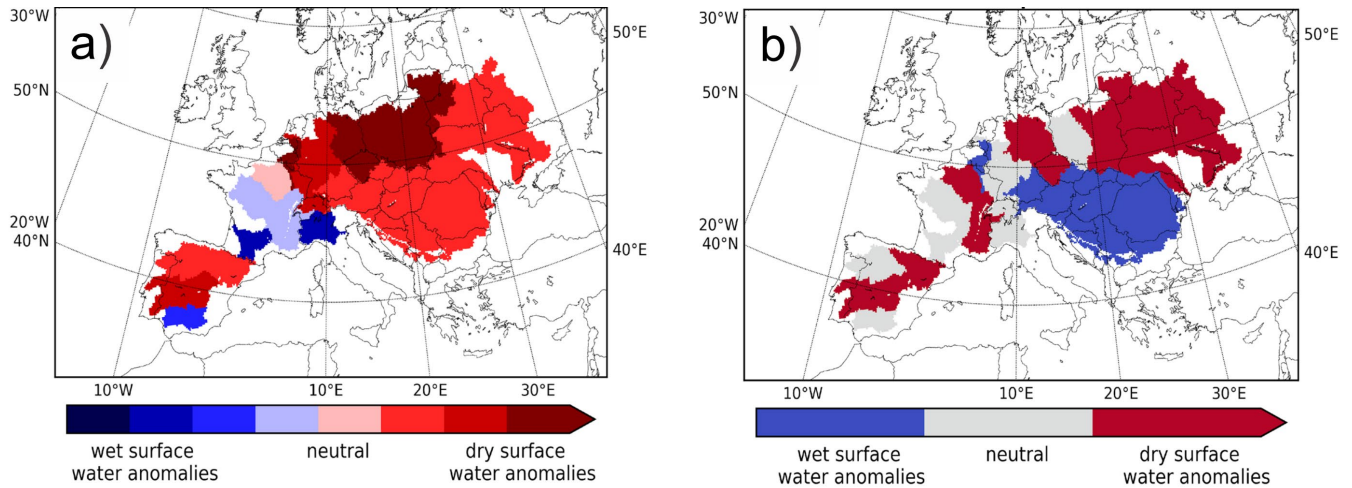
357 **Figure 2: Top: Extreme Pattern Index (EPI) for T2m surface temperature (EPIT2m, red) and precipitation deficit (EPIPd, orange)**  
 358 **for northern Hemisphere 2018 summer months. Values exceeding the 80th percentile are considered to identify extreme events in**  
 359 **PD and T2m from EPI and are highlighted in red/orange, respectively. Bottom left: second (a, b) and third (c, d) singular vectors**  
 360 **(CVs) associated with large-scale temperature (blue/red) and precipitation deficit (green/orange) pattern. Bottom right: second (a,**  
 361 **b) and third (c, d) expansion coefficient for northern hemisphere 2018 summer months. Positive values are plotted in red/orange**  
 362 **and negative values in blue/green.**

363

### 364 3.1.3 Surface water storage of the dry summer of 2018

365 The high temperature in 2018 was mainly due to increases in the amount of net surface radiation caused by the clear skies  
 366 associated with reduced precipitation (Liu et al., 2020). Germany experienced a strong increase of net radiation of  
 367 approximately +31%. Liu et al. (2020) report that land cover played a critical role in determining the occurrence and strength  
 368 of soil moisture-temperature coupling, i.e. cropland/grassland depletes soil moisture more readily than forests, thereby  
 369 triggering a more rapid release of sensible fluxes a major feature observed during the 2018 heatwave. During the 2018  
 370 heatwave, because of different soil moisture conditions, latent flux in Germany decreased by 12% and sensible flux  
 371 significantly increased by 122% (Liu et al. 2020). Further, Bastos et al. (2020) used 11 vegetation models and showed that  
 372 spring conditions promoted increased vegetation growth, which, in turn, contributed to fast soil moisture depletion, amplifying  
 373 the summer drought. Figure 3 presents the groundwater memory in the summer 2019 of the ensuing hydrological year  
 374 2018/2019 for each of the 20 European river basins on the following year's summer surface water storage ( $S_u$ ). The ensemble  
 375 simulations indicate that following the 2018 drought the conditional probability that the autumn of the hydrological year  
 376 2018/2019 (August to November 2018) is anomalously dry  $p(S_{u,d})$  is 95.5% with a  $100 \pm 0.0\%$  confidence with respect to the  
 377 climatological variability. In the following seasons,  $p(S_{u,d})$  and the associated confidence decrease due to the increasing  
 378 influence of the uncertainty in the atmospheric conditions. Specifically, for winter  $p(S_{u,d})$  is 81.8% with a confidence of  $99.5$   
 379  $\pm 0.3\%$ , for spring (March to May 2019) 63.6% with a confidence of  $80.2 \pm 6.0\%$  and for summer (June to August 2019) of  
 380 the hydrological year 2019/2020  $p(S_{u,d})$  is 68.2% with a confidence of  $90.1 \pm 3.7\%$  with respect to the climatological variability.  
 381 Without considering the groundwater storage memory effect, a probability of a dry surface water anomaly  $p(S_{u,d})$  of  $\sim 50\%$   
 382 would be expected due to the atmospheric uncertainty accounted for in the ensemble of realisations at the interannual time

383 scale. Taking drought as a precondition for  $S_u$  on this scale, the analysis shows that even one year later a  $p(S_{u,d})$  of 68% is still  
 384 well above 50% at a confidence level of  $90 \pm 4\%$ . Thus, statistically, groundwater storage takes longer than a year to fully  
 385 recover from a drought influencing surface water storage, independent of the ambient atmospheric conditions (Lorenz et al.,  
 386 2010; Orth and Seneviratne, 2012; Song et al., 2019). Recent evidence points to the fact that the impact of global warming on  
 387 soil moisture drought severity in west-central Europe such as the case in 2018 is increased. The drought risk is strongly  
 388 enhanced by the drought intensification and increase in frequency, yielding shorter recovery time between events for nature  
 389 and society (Aalbers et al., 2023).

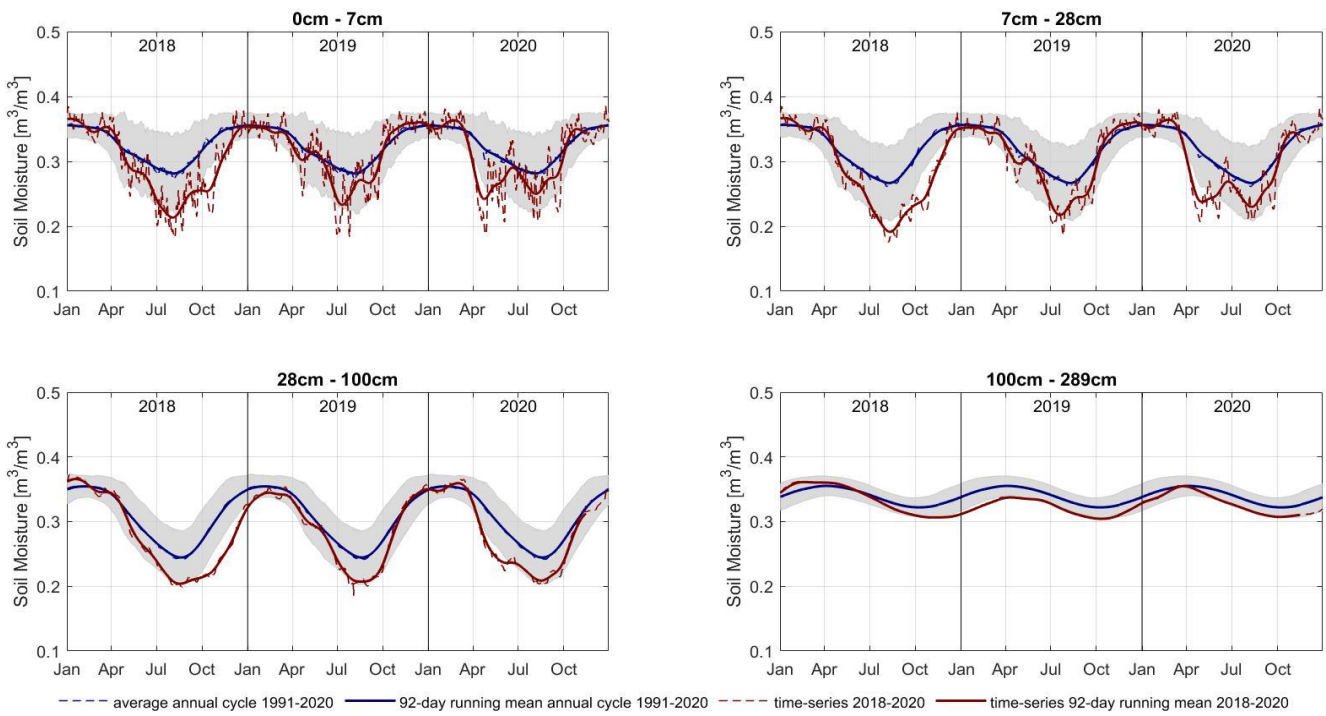


390  
 391 **Figure 3: Averaged impact of the yearlong 2018 drought on the following year's summer (June to August 2019) surface water storage**  
 392 **( $S_u$ ) anomaly per river basin (see Methods section 2.3). a)  $S_u$  anomaly in 2018 for each river basin in quartiles; b)  $S_u$  anomaly in the**  
 393 **summer (June to August 2019) after 2018 initial conditions and (ensemble) mean of 22 atmospheric conditions.**

394

### 395 3.1.4 Soil moisture of the dry summer of 2018

396 To address sectoral impacts (e.g. Conradt et al., 2023), we focus on the effects of the 2018 drought on agriculture and forestry  
 397 in Germany. For this purpose, the temporal evolution of soil moisture deficits at different depths from the ERA5 dataset and  
 398 agricultural data from German national institutes such as the Statistisches Bundesamt (Destatis) are analysed. Focusing on the  
 399 temporal evolution of soil moisture, a deficit developed during the spring and early summer of 2018 (Rousi et al., 2023), which  
 400 also reached the lowest soil layer with a temporal delay of about three months, as shown in Fig. 4. The dryness in 2018 was  
 401 more intense than the usual soil moisture variability in the period 1991-2020, as shown by the soil moisture dropping below  
 402 the range of  $\pm 1$  standard deviation of the 1991-2020 mean soil moisture (shaded area). While the moisture in the three upper  
 403 soil layers mostly recovered during the following winter 2018/2019, the moisture did not percolate down to the lowest soil  
 404 layer, which remained in a dry anomaly. The recurrent drying of the upper layers in spring and summer 2019 inhibited  
 405 considerable infiltration, so that the moisture deficit of the lower soil layer persisted until winter 2019/20, when the relatively  
 406 wet climatic conditions allowed a recharge of the lower soil layer moisture reservoir (Brakkee et al., 2022) and thus probably  
 407 also of the groundwater (e.g., Brauns et al., 2020). Hence, the lack of soil moisture reached the entire soil column and thus the  
 408 entire root zone of the vegetation during the summers of 2018 and 2019, placing the vegetation under soil moisture stress  
 409 (Tijdeman and Menzel, 2021).



410

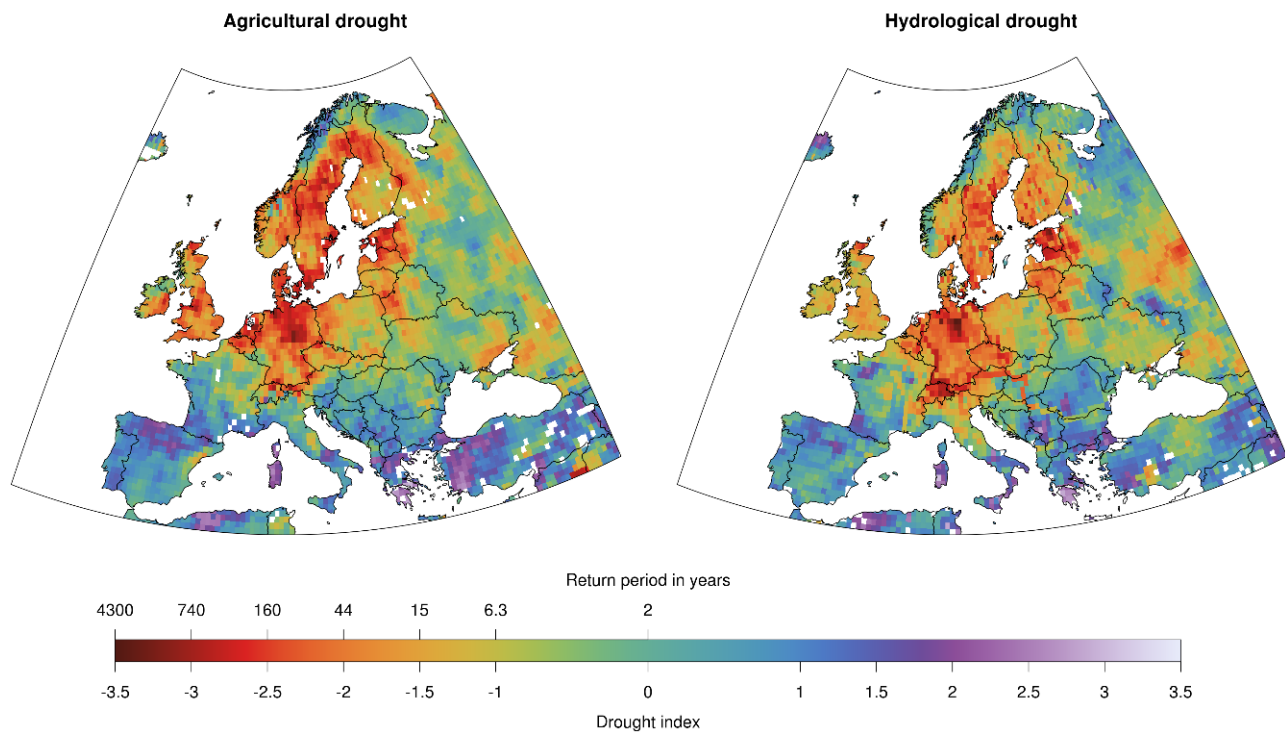
411 **Figure 4: ERA5 soil moisture in four different layers from surface (0 - 7 cm) to a depth of 2.89 m (100 - 289 cm) with two intermediate**  
 412 **layers 7 - 28 cm and 28 - 100 cm depth. The red dashed line denotes the daily mean and the solid red line denotes the 92-day running**  
 413 **mean in 2018-2020. The annual cycle of soil moisture with a daily resolution (dashed blue line) and the average running mean (solid**  
 414 **blue line) are also shown. The grey shading indicates a range of  $\pm 1$  standard deviation of soil moisture over the period 1991-2020**  
 415 **indicating the normal year-to-year variability of the soil moisture.**

416

### 417 3.1.5 Agricultural and hydrological drought of the year 2018

418 The anomalous soil moisture conditions are reflected in an anomalous low ET/PET ratio over the summer months (June, July,  
 419 August), indicating a severe agricultural drought (Fig. 5, left). In almost the entire northern part of Germany, the agricultural  
 420 drought index exceeds -2.5, which is equivalent to a return period of more than 160 years, an estimate associated with  
 421 uncertainties. However, the agricultural drought is not limited to northern Germany but comprises large parts of central,  
 422 northern, and northeastern Europe. The low soil moisture conditions also lead to a hydrological drought (low river flow) over  
 423 the summer months (Fig. 5, right). However, the severity and spatial pattern of hydrological drought differs from the pattern  
 424 of agricultural drought because propagation from soil moisture drought to hydrological drought takes time and typically leads  
 425 to a lagged occurrence (Van Loon and Van Lanen, 2012) and a longer persistence (see section 3.1.3 on Surface water storage).  
 426 Another reason is that hydrological drought can spread along the river network affecting regions unaffected by low soil  
 427 moisture (e.g., along the Danube River in eastern Europe). Nevertheless, in many parts of Germany and northern Europe,  
 428 agricultural and hydrological drought coincided in the summer of 2018 (Blauhut et al., 2022), affecting the possibility to  
 429 irrigate as a means to alleviate the agricultural drought. This provides an example of how co-occurring impacts (droughts) can  
 430 amplify each other to cause even greater secondary impacts (agricultural yields, see section 3.1.6 on Impact on the agricultural  
 431 production) in a similar way as co-occurring meteorological conditions trigger CEs.





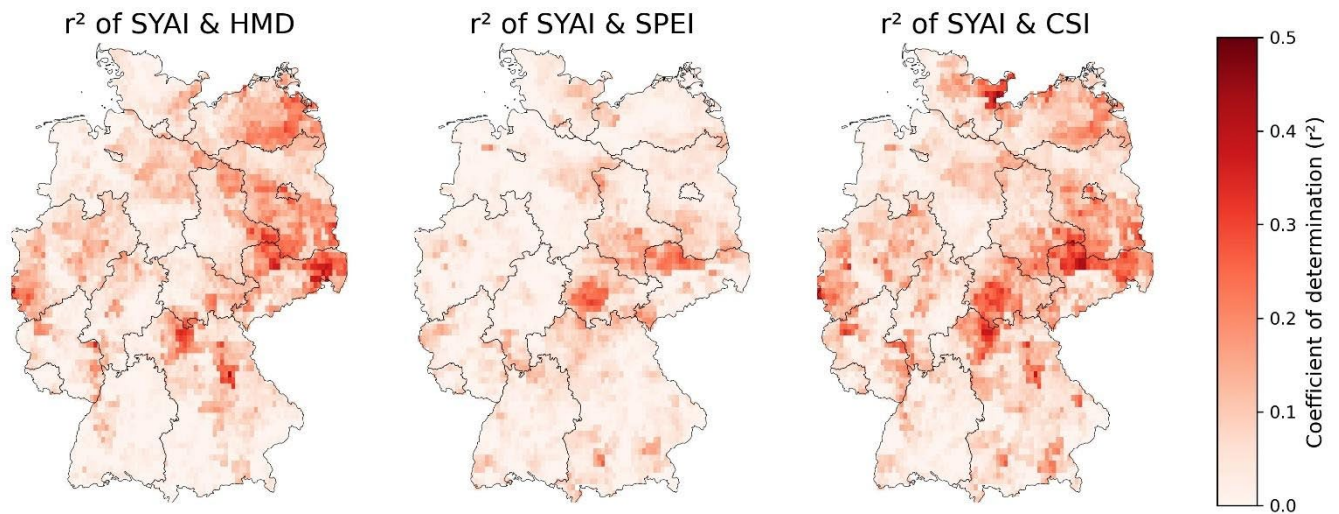
432

433 **Figure 5: Drought severity and return period of agricultural and hydrological drought during summer 2018. Note that drought**  
 434 **severity (as expressed by the drought index) and return period are closely related (see Methods section 2.5).**

435

### 436 3.1.6 Impact on the agricultural production of 2018

437 In Germany, the hot and dry spring and summer of 2018 had an unprecedented impact on crop yields. Extremely low crop  
 438 yields (Toreti et al., 2019a; Bellouin et al., 2020; Conradt et al., 2023 for northeastern Germany) led to large insurance claims  
 439 over agricultural losses and financial support requests by farmers from governments in Germany (EUR 340 million), Sweden  
 440 (EUR 116 million) and Poland (EUR 116 million) (D'Agostino, 2018; Munich Re, 2019). Winter wheat yields were more than  
 441 10% below the 30-year average and 13% below the previous three years. In some counties, yields were more than 40% lower  
 442 than in previous years. Regionally, winter wheat was particularly hard hit in eastern and northeastern Germany, with an average  
 443 loss of 22% compared to the last three decades. The HMD index and the SPEI indicate a severe heatwave and drought  
 444 respectively, which was most pronounced in central and northeastern Germany. Figure 6 shows the explained variance of yield  
 445 anomalies and the stress indices HMD, SPEI and CSI (see Methods section 2.6) revealing a strong connection between these  
 446 components. However, not all regions experienced such severe yield losses; winter wheat yield in southwest Germany was  
 447 hardly affected, with losses of only 1.2% compared to the last three-decade average. A hydrological see-saw with rather wet  
 448 conditions in southern Europe and the resulting yield increases characterise the unique combination of climatic anomalies in  
 449 Europe in 2018 (Toreti et al., 2019a). Winter wheat productivity was even positively affected in some regions.



450  
 451 **Figure 6: Coefficient of determination of Standardized Yield Anomaly Index (SYAI) and stress indices Heat Magnitude Day (HMD),**  
 452 **Standardized Precipitation Evapotranspiration Index (SPEI) and Combined Stress Index (CSI) demonstrate the impact of heat,**  
 453 **drought and compound stress over the last three decades on winter wheat in Germany.**

454  
 455 **3.1.7 Impact on the forests in 2018**

456 The drought of 2018 was likely the largest source for severe forest disturbance in Europe for more than 170 years (Senf and  
 457 Seidl, 2021), especially in central and northern Europe (Buras et al., 2020). Consequently, in the summer of 2018, about 11%  
 458 of the central European forest area experienced early wilting (Brun et al., 2020), resulting in a large reduction in greenness  
 459 (Schuldt et al., 2020; the three aforementioned studies are based on NDVI data). The 2018 drought continued into 2019, making  
 460 the consecutive European droughts of 2018 and 2019 unprecedented in the last 250 years (Hari et al., 2020). The low soil  
 461 moisture content in 2018 and an increased water-vapour pressure deficit in the following two years were the main drivers for  
 462 the forest disturbances of about  $4.74 \times 10^6$  ha in Central Europe (Senf and Seidl, 2021). The likely cause for these forest  
 463 damages was that trees under drought and heat stress experience carbon starvation (Bastos et al., 2020) and have risk for  
 464 embolism, which causes failures in water transport (Allen et al., 2015; Schuldt et al., 2016). The drought and heatwave in that  
 465 period facilitated outbreaks of bark beetle, enhancing the damage levels to forests. As such, insect outbreaks in Central Europe  
 466 had a 2-3-fold increase in annual losses between 2017 and 2018 (Hlásny et al., 2019) and extraordinary mortality and damage  
 467 occurred during 2018 in Sweden due to rapid beetle population growth (Öhrn et al., 2021). Although wildfires have decreased  
 468 on a global scale recently, Central Europe is likely to face larger and more frequent forest fires (Feurdean et al. 2020, Milanovic  
 469 et al. 2020; Carnicer et al., 2022), which can have severe environmental, economic and social consequences (Lidskog et al.  
 470 2019).

471 **3.2 Precipitation-wind compound events during 2018**

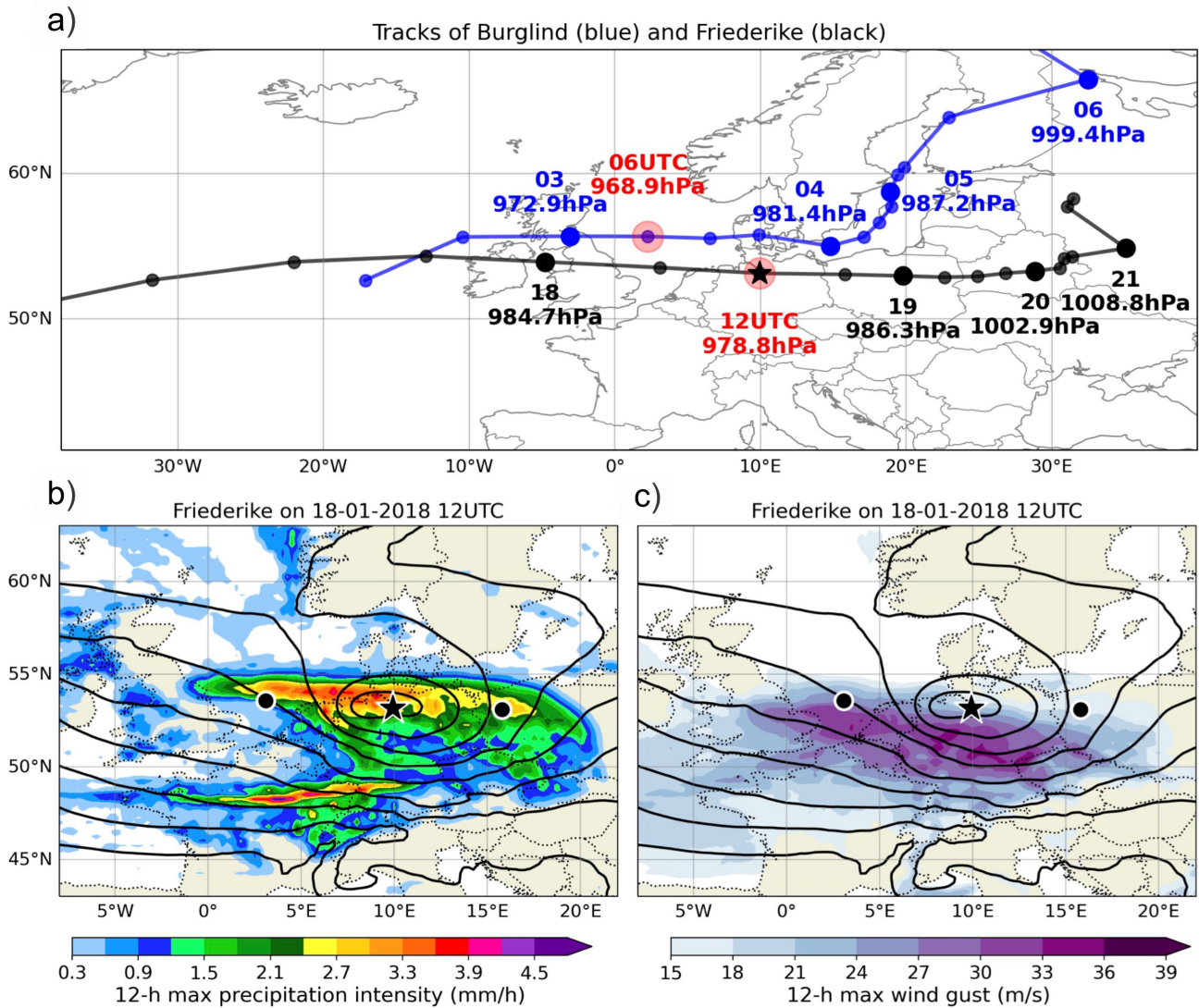
472 In this section, CEs that involve heavy precipitation and strong winds are described. Examples include two January windstorms  
 473 (Friederike and Burglind) and several weeks of convective activity in May and June of 2018.

474 **3.2.1 Loss and damage of compound vs. non-compound wind extreme events of the winter 2018**

475 On January 16, windstorm Friederike formed as a low-pressure system near Newfoundland. Within the next two days,  
 476 Friederike intensified and quickly travelled across the Atlantic (Fig. 7), losing its closed structure at 1800 UTC on 17 January.  
 477 Friederike re-intensified over the British Isles on 18 January while crossing the jet streak towards the northern jet exit region,  
 478 a behaviour favourable for intense windstorm development (e.g., Pinto et al., 2009). The storm moved eastward over the North

479 Sea, Germany and Poland, and weakened after 19 January over eastern Europe (Fig. 7a). Analysing the compound character  
480 of Friederike around peak intensity using the hourly ERA5 reanalysis data (Fig. 7b,c), the typical near-surface wind and  
481 precipitation structure of intense extratropical cyclones is found (e.g., Dacre et al., 2012). Strong 10 m wind gusts (maximum  
482 values of 34 m/s relative to the Earth's surface) were present behind and to the right of the eastward moving cyclone centre.  
483 Heavy precipitation occurred at both the warm front to the northeast of the centre, wrapping around as the cyclone approached  
484 its mature stage, and along the east-southwest stretching cold front (Fig. S1a). During the 12 h period when Friederike passed  
485 through Germany from 0600 UTC to 1800 UTC on 18 January, the persistently active warm front left a widespread footprint  
486 near the northern edge of the cyclone centre (Fig. 7b) with ERA5 accumulated precipitation exceeding 17 mm. Meanwhile,  
487 the cold front contributed to a high precipitation rate ( $> 4$  mm/h based on ERA5) along a narrow west-east oriented band across  
488 northern France and southern Germany (Fig. 7c). The co-occurrence of strong winds and heavy snowfall gave to this storm  
489 the risk and damage characteristics of a CE (Fig. 7b,c). The highest damages were reported in Ireland, Great Britain, northern  
490 France, Belgium, the Netherlands, Germany, Czech Republic and Poland, where gust measurements suggested wind speeds of  
491 the order of 100 – 150 km/h. At higher altitudes the observed wind gusts reached 173 km/h at the Sněžka in Czech Republic  
492 and 203 km/h at Brocken in Germany (Haeseler et al., 2018). Wind and snowfall associated with Friederike caused further  
493 traffic disruption, power outages, property damage including falling trees, and several deaths. Friederike was the strongest  
494 storm affecting central Germany since windstorm Kyrill in 2007.

495 Another CE affecting Germany in the same month was the windstorm Burglind, which formed on the 2nd January 2018. The  
496 depression intensified rapidly as it moved eastwards towards the British Isles (Fig. 7a). It reached a peak intensity of 968.9  
497 hPa at 0600 UTC on 3 January 2018 over the North Sea, followed by a weakening over the Baltic Sea. The long active cold  
498 front affected a large area of western Europe (Fig. S1b). Heavy precipitation with daily values  $> 30$ mm led to rapid snowmelt  
499 and massive flooding in many regions. Around the time of the peak cyclone intensity, widespread areas were simultaneously  
500 affected by high precipitation intensities ( $> 4$  mm/h) and high wind gust ( $\sim 100$ km/h) (Fig. S1c,d). Further detailed information  
501 on Burglind can be found in Eisenstein et al. (2022, see their section 5). Compared to storm Friederike, the compound features  
502 of Burglind were more strongly shaped by orography.



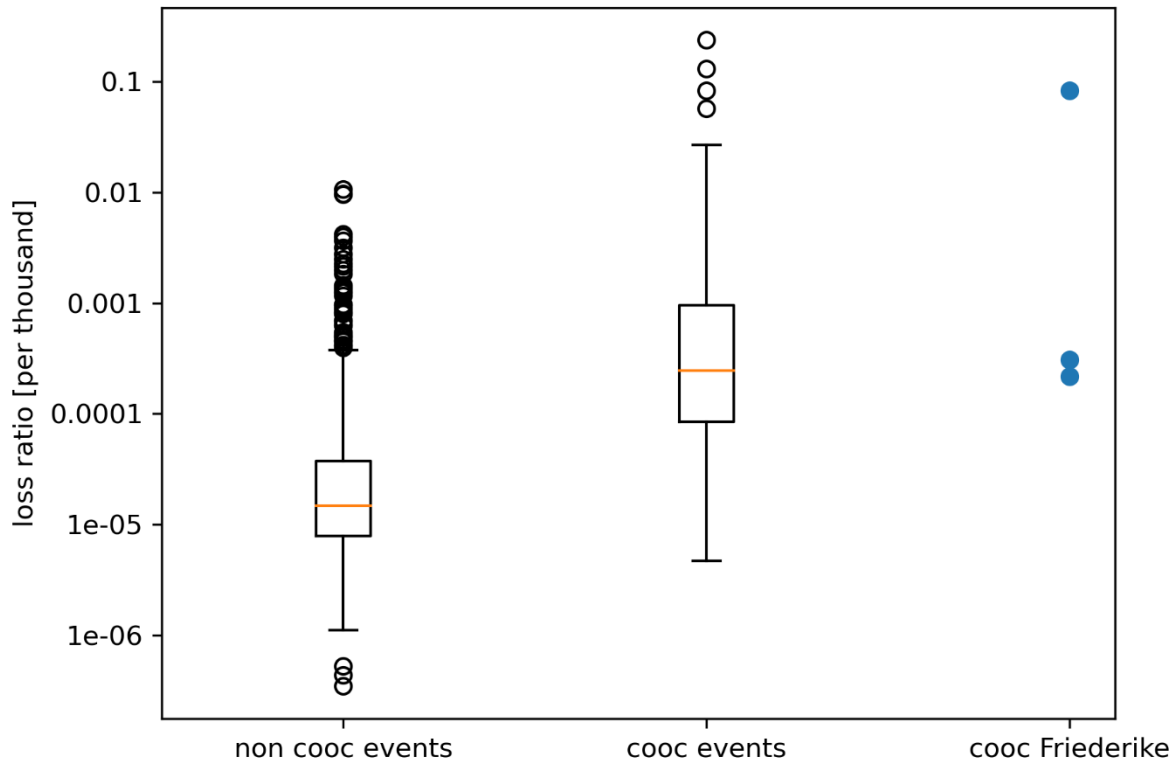
503

504 **Figure 7: a) Cyclone tracks of windstorms Friederike (black) and Burglind (blue) in January 2018. Big circles show locations at 0000**  
 505 **UTC on the day as indicated, with the central pressure noted below. Red circles indicate their lifetime peak intensity based on the**  
 506 **minimum pressure. b) Mean sea level pressure (thick contours; increasing from 960 hPa with 5 hPa intervals) at 1200 UTC on 18**  
 507 **January 2018 (location of Friederike shown by the star) and maximum precipitation intensity (shaded) during the period 6 h before**  
 508 **and after (locations shown by black circles). c) Same as b), but for the wind gust at 10 m height (shaded). All fields are derived from**  
 509 **the ERA5 reanalysis (Hersbach et al., 2018).**

510

511 Although the co-occurrence of extreme wind and precipitation is discussed in previous studies for specific events (e.g. Fink et  
 512 al., 2009 for storm Kyrill) or globally (Martius et al., 2016; Messmer and Simmonds, 2021), there are no studies so far  
 513 quantitatively evaluating the effect in terms of loss damage. To distinguish between single extreme wind speed events and  
 514 compound extreme wind speed and precipitation events, we follow the definition of Martius et al. (2016), where both variables  
 515 are considered simultaneously (see the Methods section 2.7). The loss damage distribution for compound and non-compound  
 516 events determined from loss data of the GDV is depicted in Fig. 8. For Friederike, there are three days where a co-occurrence  
 517 of wind and precipitation extremes can be identified over Germany, i.e. 17, 18, and 19 January 2018. The loss ratio for these  
 518 three days is marked with blue dots in the right column of Fig. 8. The GDV Naturgefahrenreport (2019) reports 900 million €  
 519 loss damage for Germany with respect to Friederike. To this date, it was the most damaging winter storm of the last ten years.





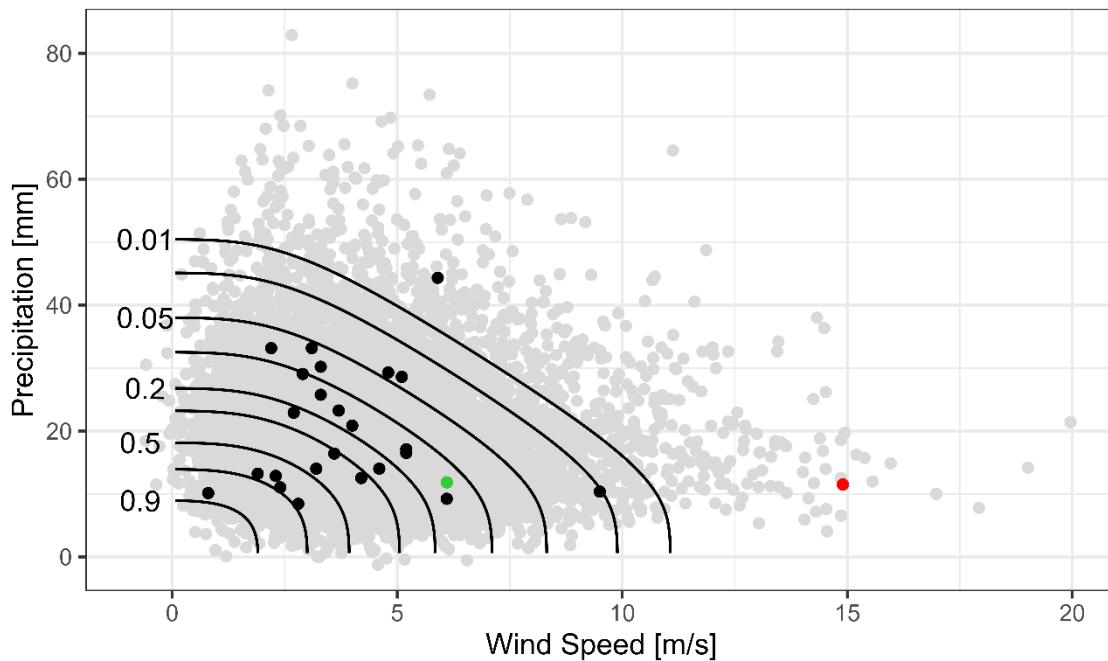
520

521 **Figure 8: Loss ratio of residential buildings [per thousand] accumulated over Germany for winter events from 1997-2016. Each dot**  
 522 **represents one day. Left (non cooc events) bar shows all days which cannot be linked to co-occurrence (cooc) of both extreme wind**  
 523 **and precipitation, i.e. single extreme events. Middle bar (cooc events) shows all days which can be linked to co-occurrence of extreme**  
 524 **wind and precipitation. Right bar shows the three days for the co-occurrence during windstorm Friederike. The loss ratio is defined**  
 525 **by loss normalized with the local sum of insured values.**

526

### 527 3.2.2 Concurrent heavy rain and storm extremes – estimation of probability of event occurrence

528 In a detailed analysis of the probability of co-occurrence of extremes, based on copulas (see Methods section 2.8), the annual  
 529 maximum values of hourly precipitation and wind speed data at the station Münster/Osnabrück Airport of DWD that are  
 530 available since 1996 were analysed. The records show an increase in the intensity and frequency of the variables but lack a  
 531 statistically significant trend. The occurrence probabilities for concurrent precipitation and wind extreme events are shown by  
 532 the black isolines in Fig. 9. The grey dots are pseudo-observations (artificial precipitation and wind combinations generated  
 533 using the copula function), while the black, red and green dots mark the observed CEs at the station for each year and the green  
 534 dot represents Friederike. The distribution of the dots illustrates that - depending on the precipitation duration - wind or  
 535 precipitation, individually, may not be extreme. A counterexample is the year 2020 windstorm Sabine (red dot; internationally  
 536 known as Ciara) for which the simultaneous wind and hourly precipitation values both correspond to the respective annual  
 537 maximum event of that year. The location of the dots relative to the isolines define the return period of the event, where the  
 538 return period of windstorm Friederike at the station Münster/Osnabrück exceeded 5 years and the one of windstorm Sabine  
 539 100 years.



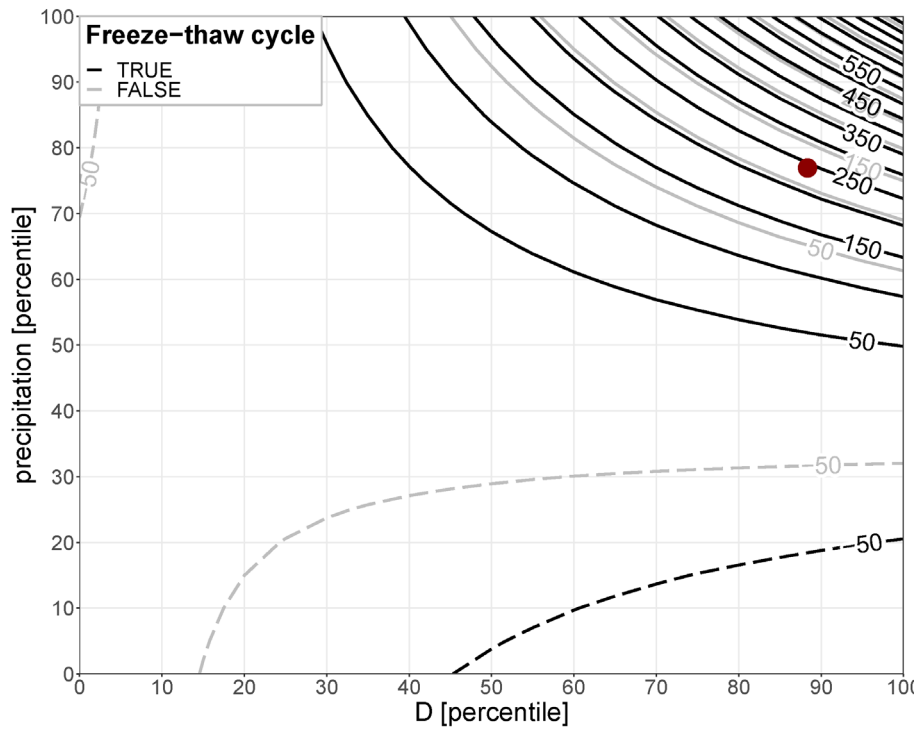
540

541 **Figure 9: Multivariate analyses for the temporal compound event heavy precipitation and strong wind determined with Copula**  
 542 **functions: quantile isolines (lines of equal probabilities), observed event combinations (black dots) and the pseudo-observations (grey**  
 543 **dots). Green dot represents storm Friederike (2018) and red dot storm Sabine (2020).**

544

### 545 3.2.3 Rockfall events

546 Another hazard with CE triggers observed in connection with Friederike was a rockfall event. Although wind is normally not  
 547 considered as one of the triggering factors (D'Amato et al., 2016), such events may also occur as the consequence of the  
 548 precipitation associated with the windstorm. It is well known that heavy precipitation can initiate landslides and rockfall events  
 549 (e.g. Nissen et. al., 2022). Slope susceptibility is influenced by pore water/fissure water preconditions, rendering them events  
 550 with multivariate and temporally compounding triggers. With respect to rockfall, another potentially triggering factor are  
 551 freeze-thaw cycles prior to the event. In terms of reported hill slope failures, storm Burglind was more effective than storm  
 552 Friederike. For storm Friederike, only one rockfall event is registered in the landslide database for Germany. The event  
 553 occurred near Göttingen in Lower Saxony. Figure 10 shows the relationship between the predictors (across-site percentile of  
 554 a fissure water proxy  $D$ -precipitation minus potential evaporation determined for the last 5 days-, the local percentile of daily  
 555 precipitation and the binary information if a freeze-thaw cycle occurred within the last 9 days) and the rockfall probability  
 556 expressed as percentage change with respect to the climatological probability. The red dot indicates the conditions on the 18th  
 557 January 2018 in the area of the event associated with Friederike. The soil at the location was still wet after storm Burglind at  
 558 the beginning of month and the fissure water (proxy  $D$ ) at its 83rd percentile. The daily precipitation on the day of the event  
 559 was 4.5 mm (REGNIE data, Rauthe et al., 2013), which corresponds to the 77th percentile for the given location, assuming  
 560 immediate melting of the reported snow due to the above freezing air temperature at the event location. The probability of a  
 561 rockfall event was further increased by pre-event thawing conditions. The logistic regression model suggests that the  
 562 probability of rockfall on that day was increased by almost 250% (3.5 times more likely) compared to the long-term  
 563 climatology.



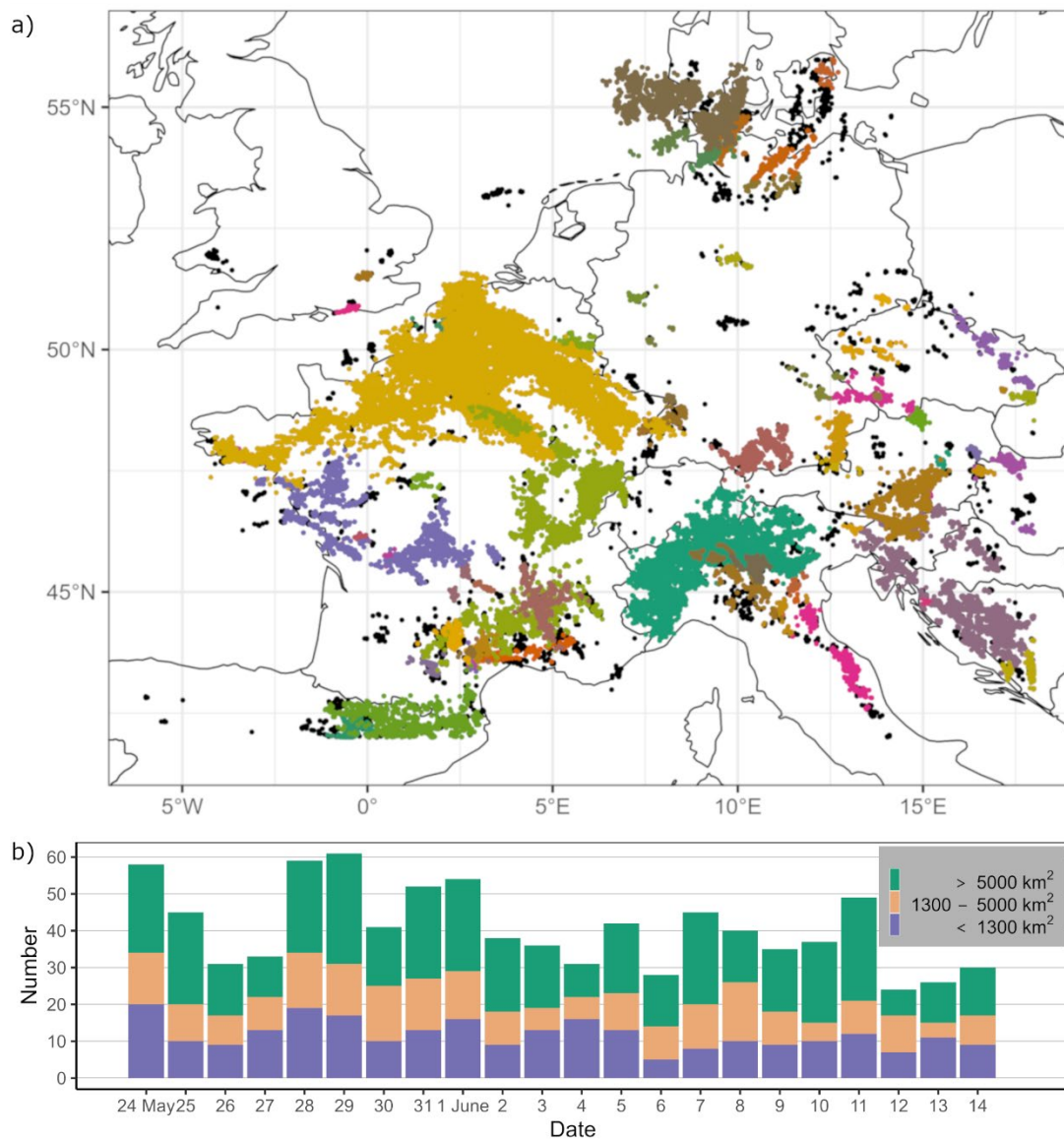
564

565 **Figure 10: Rockfall probability expressed as percentage change with respect to the climatological probability (isolines) as a function**  
 566 **of moisture preconditions (D), daily precipitation and preceding freeze-thaw cycles (see Methods section 2.9). The red dot marks the**  
 567 **conditions in the vicinity of Göttingen (Lower Saxony) on 18th January 2018.**

568

569 **3.2.4 Convective cluster events of the summer 2018**

570 The spatially as well as temporally compounding nature of severe convective storms (SCSs) can be demonstrated on the  
 571 example of a three-week series of SCSs in western and central Europe from 22 May to 12 June 2018 leading to the unusual  
 572 high temporal accumulation of CCEs lasting several days (Fig. 11). During this period, an exceptional persistence of reduced  
 573 stability combined with sufficient moist air masses caused high thunderstorm activity daily in France, Belgium, Netherlands,  
 574 Luxembourg, Germany, Switzerland, and/or Austria, associated with precipitation accumulations of up to 80 mm/h within 1  
 575 hour and several flash floods (Mohr et al., 2020). The temporal compounding nature of the serial clustering of SCSs over  
 576 several days to weeks over the same geographic region may increase the probability of flooding and damage. Figure 11b shows  
 577 a large amount of identified CCEs, especially those with large spatial extent (> 5000 km<sup>2</sup>), during a three-week period over  
 578 western and central Europe indicating high thunderstorm activity whose accumulation was unusual (Piper et al., 2016; Mohr  
 579 et al., 2020). The repeating occurrence is caused by persistent synoptic conditions that favour thunderstorm development over  
 580 several days to weeks. The presence of atmospheric blocking has been found to be highly conducive to such prolonged  
 581 thunderstorm episodes, which typically occur on its western and /or eastern flanks (Piper et al., 2016; Mohr et al., 2020; Kautz  
 582 et al., 2022). Based on statistical analyses, Mohr et al. (2019) found that a block over Scandinavia or over the Baltic Sea  
 583 favoured the occurrence of thunderstorms in western and central Europe along the western flank of the blocking system due  
 584 to of southwesterly advection of warm, moist, and unstable air masses. It is expected that low-frequency modes of climate  
 585 variability like North Atlantic Oscillation (NAO) or East Atlantic Pattern (EA) could also have an impact on clustered  
 586 thunderstorm activity over several days (Piper et al., 2019), as these patterns are connected with atmospheric blocking.



587

588

589

590

591

592

593

#### 4 Compound events under climate change

594

595

596

597

598

599

600

601

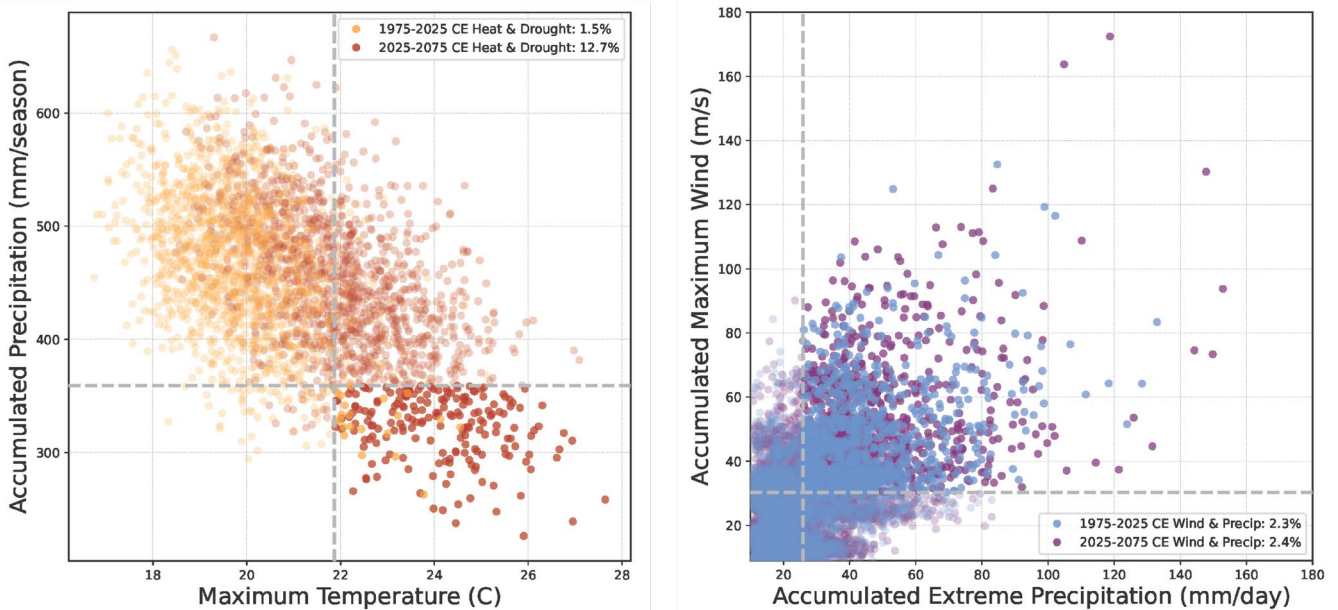
602

603

604

In this paper, we have analysed in detail several extreme events that have affected Europe within the calendar year of 2018, starting with the windstorm series in January, followed by a period of heavy thunderstorms in May/June and extended heatwave in July and August which affected various parts of Europe, and the associated drought effects extended well into the autumn season. Our analysis clearly revealed the multivariate and complex characteristics of the events, and thus they can undoubtedly be classified as CEs. The analysis of compound variables was used as a tool to investigate the impacts of man-made climate change. For the two overarching compound types collected in this contribution (hot and dry; wet and windy) we now analyse possible changes of their frequency of occurrence under future climate conditions. Recent studies have provided evidence that regionally extreme hot and dry conditions such as the summer 2018 are expected to become more frequent in the future (e.g., Toreti et al. 2019a; Zscheischler and Fischer, 2020; Aalbers et al., 2023; van der Wiel et al., 2021; Bevacqua et al., 2023). Figure 12 shows a comparison of the occurrence of CEs under recent (1975-2025) climate conditions, with a global mean surface temperature of 1 °C above pre-industrial levels, and under future (2025-2075) conditions of 3 °C above pre-industrial

605 levels, based on the 30-member CMIP6 MPI-GE under SSP5-8.5 (see Methods section 2.11). For drought and heat events, our  
 606 analysis reveals a clear increase in both the frequency and intensity of extreme compound heat and drought years (Fig. 12,  
 607 left). Over the past 50 years, extreme compound heat-drought events have occurred with a probability of 1.5%, or about 1-2  
 608 times per century. Over the next 50 years, such extreme CEs are projected to become almost 10 times more frequent, occurring  
 609 more than once every 10 years, and reaching much higher temperatures and precipitation deficits.  
 610 The likelihood of winters with extreme compound precipitation-strong wind events does not change significantly with global  
 611 warming in the CMIP6 MPI-GE projections (Fig. 12, right). Such wet and windy winters, where both precipitation and wind  
 612 are extreme, are projected to occur about once every 50 years. However, although the number of projected events remains  
 613 roughly the same, the intensity of the actual wind and precipitation levels reached during the most extreme compound wet-  
 614 windy events increases substantially in the near future.

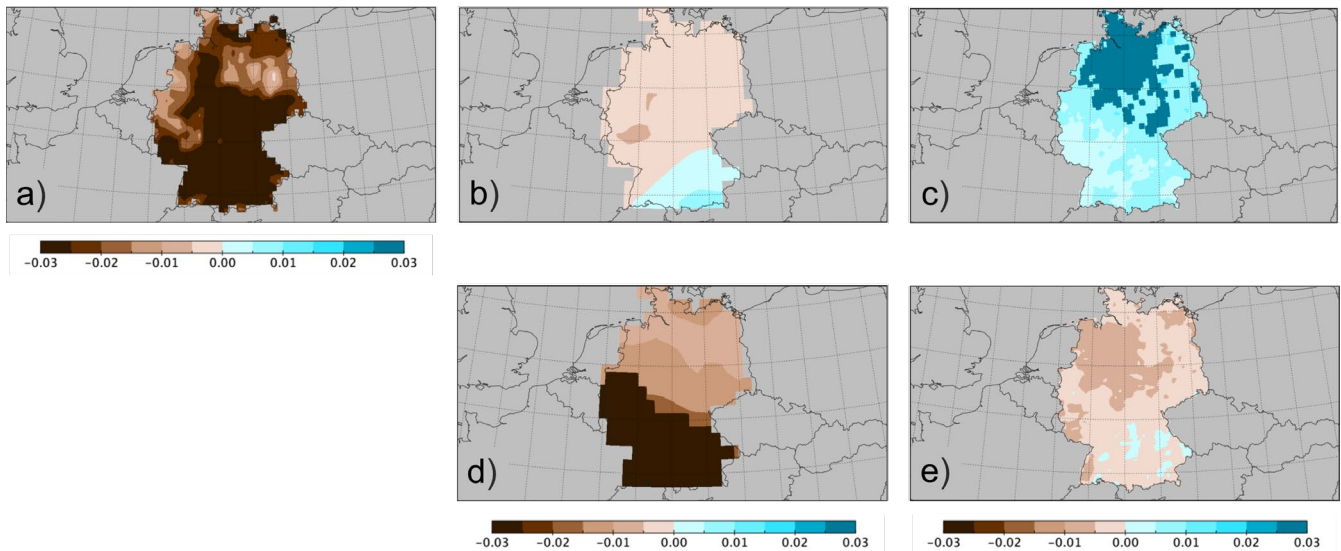


615  
 616 **Figure 12: Changes of temperature-precipitation (heat-drought, left) and precipitation-wind (wet-windy, right) compound years**  
 617 **occurrence in terms of frequency and intensity, at 1 °C (1975-2025) and 3 °C (2025-2075) above the pre-industrial levels based on**  
 618 **the 30-member CMIP6 MPI-GE under SSP5-8.5 (Olonscheck et al., 2023) over Germany.**

619  
 620 A factor that strongly modulates the occurrence of extremes in Europe is the soil moisture availability, as decreasing soil  
 621 moisture availability initiates a suite of processes feeding back into an intensification of both heat waves and droughts (Miralles  
 622 et al., 2019). Figure 13 presents a comparison between the observed (ERA5), simulated (extended historical) and projected  
 623 (RCP8.5) drought conditions via the SPEI moisture availability index (see Methods section 2.12). For the historical period  
 624 1979-2019, the reanalysis shows trends in the 3-year running mean SPEI, with a clear drying tendency in central and southern  
 625 Germany during the warm season, with lower values elsewhere in Germany (Fig. 13a). Part of this trend may be related to the  
 626 multi-year drought of 2018-2020 at the end of the time series. The CMIP5 multi-model ensemble under observed (extended  
 627 historical) greenhouse gas concentrations (Fig. 13b) fails however at depicting the trends for the past decades, while Euro-  
 628 CORDEX (Fig. 13c) simulates an increased water availability across Germany. The future projections following the RCP8.5  
 629 scenario are roughly consistent between CMIP5 (Fig. 13d) and EURO-CORDEX (Fig. 13e). Both ensembles predict a  
 630 considerable trend towards more impactful multi-year drought conditions under RCP8.5. Differences between the various  
 631 sources of data may be related to specific characteristics and settings of the climate models, such as the treatment of  
 632 anthropogenic aerosols, the inherited uncertainty and bias of climate models to replicate the precipitation variability at the  
 633 regional and local scale, the differences of the convective precipitation during the warm part of the year (Dyrrdal et al., 2017),  
 634 but also the use of multi-model ensembles that may mask the individual model skill (Ridder et al., 2022). These examples  
 635 demonstrate the need for further model development to improve their ability to accurately reproduce observed CEs and their



636 characteristics, thus reducing the uncertainty of future projections and contributing to improved prevention, risk management  
637 and future preparedness.



638  
639 **Figure 13: Decadal trends, 1975-2021 and 2022-2077, of the 3-yr running mean Standardised Precipitation Evapotranspiration Index**  
640 **for a) ERA5, b) historical CMIP5 multi-model ensemble extended by Aalbers et al. (2023), c) EURO-CORDEX multi-model**  
641 **ensemble, d) RCP8.5 CMIP5 multi-model ensemble and e) RCP8.5 EURO-CORDEX multi-model ensemble. Significant model**  
642 **ensemble grid points are shaded dark brown and dark green. Units are standard deviation for spring and summer.**

643

## 644 5 Conclusions – Lessons learned and future steps

645 Compound climate events had severe impacts across Europe in 2018, as combinations of extreme weather events unfolded  
646 simultaneously or in succession, resulting in extensive socio-economic, environmental, and infrastructural damage. The study  
647 highlights two primary types of CEs: hot-dry and wet-windy, each amplifying the effects of individual weather extremes. A  
648 variety of statistical approaches and datasets have been explored and implemented, spanning different types of events and  
649 disciplines.

650 The summer of 2018 was marked by prolonged heatwaves and drought conditions across Europe, driven largely by persistent  
651 large-scale atmospheric blocking. Soil moisture declined sharply from spring through summer, imposing widespread stress on  
652 agriculture, forests, and water resources. These conditions led to significant agricultural losses, particularly in winter wheat  
653 yields, and imposed severe stress on European forests, resulting in large-scale forest fires and insect outbreaks.

654 The winter of 2018 saw a sequence of intense storms, including Friederike and Burglind, which brought strong winds and  
655 heavy precipitation, causing widespread flooding, property damage, and economic losses in multiple countries. The  
656 combination of sustained high winds and heavy precipitation further increased the risk of landslides and rockfalls, particularly  
657 in regions with saturated and thawing soils.

658 Projections indicate that, under progressing climate change, hot-dry events will increase in frequency and severity, while wet-  
659 windy events may retain similar frequencies but with greater intensity. Current adaptation and risk management strategies may  
660 be insufficient, as they often focus on single-event risks and may underestimate the compound hazards posed by concurrent  
661 extremes.

662 This study encourages further research on compound events to improve predictive capabilities and inform adaptation strategies.  
663 Integrated climate models that better represent the complex interactions of multiple extremes are crucial. Next steps involve  
664 validating the physical relationships between predictors and CEs to identify the underlying mechanisms that drive or modify  
665 these events, which could lead to more accurate analyses and predictions of CEs. Furthermore, given the complexity of CEs

666 and their direct impacts, a redefinition of events based primarily on their relevant impacts, rather than purely statistical  
667 characteristics, is necessary to effectively assess and manage these risks.

668 These findings underscore the need for comprehensive climate adaptation approaches that address the interconnected nature  
669 of compound events, ensuring more effective preparedness for the compounded risks of future climate extremes.

670

671

#### 672 **Code availability**

673 Code is available from the authors upon request.

674

#### 675 **Data availability**

676 The ERA5 (<https://doi.org/10.1002/qj.3803>, Hersbach et al., 2020) reanalysis data are publicly available via the Copernicus  
677 Climate Change Service (<https://doi.org/10.24381/cds.adbb2d47>, Hersbach et al., 2023). The gridded observational datasets  
678 E-OBS (<https://doi.org/10.1029/2017JD028200>, Cornes et al., 2018) are publicly available on the European Climate  
679 Assessment & Dataset website (<https://www.ecad.eu/download/ensembles/download.php>, ECA&D, 2023). The observational  
680 datasets (<https://doi.org/10.5194/asr-10-99-2013>, Kaspar et al., 2013) and the phenological data from the German Weather  
681 Service (DWD; <https://doi.org/10.5194/asr-11-93-2014>, Kaspar et al., 2015) are publicly available on the DWD website under  
682 their Open Data Portal (<https://opendata.dwd.de/>, DWD, 2023). The yield productivity data (Ellsäßer and Xoplaki, 2022a:  
683 <http://dx.doi.org/10.22029/jlupub-7177>), the yield anomaly catalogue (Ellsäßer and Xoplaki, 2022b:  
684 <http://dx.doi.org/10.22029/jlupub-7176>) and supplementary data (Ellsäßer and Xoplaki, 2022c,  
685 <http://dx.doi.org/10.22029/jlupub-7203>) are publicly available at the JLUpub research data repository. Historic climate data  
686 from the GSWP-W5E5 dataset used for LPJmL5 simulations are available from <https://doi.org/10.48364/ISIMIP.982724>  
687 (Lange et al., 2022). The historical data of atmospheric N deposition and atmospheric CO<sub>2</sub> concentrations can be obtained  
688 from <https://doi.org/10.48364/ISIMIP.600567> (Yang and Tian, 2020) and <https://doi.org/10.48364/ISIMIP.664235.2> (Büchner  
689 and Reyer, 2022), respectively. All input data, model code, model outputs, and post-processing scripts that have been used to  
690 produce the LPJmL-related results in this paper are archived at the Potsdam Institute for Climate Impact Research and are  
691 available upon request.

#### 692 **Competing interests**

693 At least one of the (co-)authors is a member of the editorial board of Natural Hazards and Earth System Sciences. The peer-  
694 review process was guided by an independent editor, and the authors also have no other competing interests to declare.

695

#### 696 **Author Contribution**

697 EX and FE coordinated the interdisciplinary task force on compound events within climXtreme and this collaborative paper,  
698 conducted the agriculture case study analysis with Figure 6 and methods, prepared the first and final drafts of the paper based  
699 on the contribution of the co-authors; ER contributed the drivers of the hot summer of 2018 case study with Figure 1; SS  
700 contributed the detection of spatial patterns of extreme events and Figure 2; LG and SK contributed with the surface water  
701 storage case study analysis and Figure 3; LJ contributed the soil moisture case study and Figure 4; JH contributed with the  
702 analysis of the agricultural and hydrological droughts and Figure 5; DG and FK contributed with the forestry case study; JGP  
703 and T-CC contributed the windstorms description and prepared Figure 7 and S1; JGP contributed to the compound events  
704 under climate change section; JG conducted the loss analysis for windstorms with Figure 8 and contributed to the methods  
705 section; FS conducted the copula analysis and prepared Figure 9; KNM contributed the rockfall events case study analysis  
706 with Figure 10, drafted the section on precipitation-wind compound events and contributed to the compound events under

707 climate change section; SM and MA analysed convective storms and provided Figure 11; LSG did the CMIP6 MPI-GE  
708 projection study and prepared Figure 12; KH contributed the analysis of soil moisture representation and trend in model  
709 simulations with Figure 13. NL and OV contributed to the temperature-precipitation compound events section; JL contributed  
710 drafting different sections and versions of the paper, and all authors followed the analysis from the beginning, provided text  
711 and edited/commented the final version of the manuscript.

## 712 **Acknowledgements**

713 This paper is a collaborative effort within the BMBF climXtreme project, for which the authors acknowledge funding (grant  
714 numbers 01LP1901A, 01LP1903C, 01LP1901F, 01LP1903A, 01LP1902J, 01LP1903F, 01LP1902M, 01LP1901E). EX, NL,  
715 OV acknowledge support by the EU Horizon 2020 Project CLINT under Grant Agreement number 101003876. EX  
716 acknowledges support by the BMWK project DAKI-FWS (grant number 01MK21009I) and the EU Horizon Europe project  
717 MedEWSa under Grant Agreement number 101121192. JGP thanks the AXA research fund for support. LSG has also received  
718 funding from the European Union's Horizon Europe Framework Programme under the Marie Skłodowska-Curie grant  
719 agreement No 101064940. SMVB acknowledges funding from the DFG training group NatRiskChange (grant No GRK  
720 2043/1). We acknowledge the World Climate Research Programme's Working Group on Coupled Modelling, which is  
721 responsible for CMIP, and we thank the climate modelling groups for producing and making available their model output. For  
722 CMIP the U.S. Department of Energy's Program for Climate Model Diagnosis and Intercomparison provides coordinating  
723 support and led development of software infrastructure in partnership with the Global Organization for Earth System Science  
724 Portals. We acknowledge the World Climate Research Programme's Working Group on Regional Climate, and the Working  
725 Group on Coupled Modelling, former coordinating body of CORDEX and responsible panel for CMIP5. We also thank the  
726 climate modelling groups for producing and making available their model output. We also acknowledge the Earth System Grid  
727 Federation infrastructure, an international effort led by the U.S. Department of Energy's Program for Climate Model Diagnosis  
728 and Intercomparison, the European Network for Earth System Modelling and other partners in the Global Organisation for  
729 Earth System Science Portals (GO-ESSP). We acknowledge the E-OBS dataset from the EU-FP6 project UERRA  
730 (<http://www.uerra.eu>) and the Copernicus Climate Change Service, and the data providers in the ECA&D project  
731 (<https://www.ecad.eu>).

## 732 **References**

- 733 Aalbers, E. E., van Meijgaard, E., Lenderink, G., de Vries, H., and van den Hurk, B. J. J. M.: The 2018 west-central European  
734 drought projected in a warmer climate: how much drier can it get?, *Nat. Hazards Earth Syst. Sci.*, 23, 1921–1946,  
735 <https://doi.org/10.5194/nhess-23-1921-2023>, 2023.
- 736 Allen, C. D., Breshears, D. D., and McDowell, N. G.: On underestimation of global vulnerability to tree mortality and forest  
737 die-off from hotter drought in the Anthropocene, *Ecosphere*, 6, 1-55, 2015.
- 738 Augenstein, M., Mohr, S., and Kunz, M.: Analysis of thunderstorm clusters derived from lightning data with ST-DBSCAN in  
739 West and Central Europe, *Nat. Hazards Earth Syst. Sci.*, in prep.
- 740 Barriopedro, D., Fischer, E.M., Luterbacher, J., Trigo, R.M., and García-Herrera, R.: The hot summer of 2010: redrawing the  
741 temperature record map of Europe, *Science*, 332, 220-224, 2011.
- 742 Bastos, A., et al.: Direct and seasonal legacy effects of the 2018 heat wave and drought on European ecosystem productivity,  
743 *Sci. Adv.*, 6, eaba2724, <https://doi.org/10.1126/sciadv.aba2724>, 2020.



- 744 Bastos, A., Orth, R., Reichstein, M., Ciais, P., Viovy, N., et al.: Vulnerability of European ecosystems to two compound dry  
745 and hot summers in 2018 and 2019, *Earth Syst. Dyn.*, 12:1015–1035, 2021, <https://doi.org/10.5194/esd-12-1015-2021>
- 746 Beloiu, M., Stahlmann, R., and Beierkuhnlein, C.: High Recovery of Saplings after Severe Drought in Temperate Deciduous  
747 Forests, *Forests*, 11:546, <https://doi.org/10.3390/f11050546>, 2020.
- 748 Beillouin, D., Schauburger, B., Bastos, A., Ciais, P., and Makowski, D.: Impact of extreme weather conditions on European  
749 crop production in 2018, *Philos. T. R. Soc. B*, 375, 20190510, <https://doi.org/10.1098/rstb.2019.0510>, 2020.
- 750 Bender, J.: Zur Ermittlung von hydrologischen Bemessungsgrößen an Flussmündungen mit Verfahren der multivariaten  
751 Statistik. Mitteilung des Forschungsinstituts Wasser und Umwelt der Universität Siegen, 9. [http://dokumentix.uw.uni-](http://dokumentix.uw.uni-siegen.de/opus/volltexte/2015/965/pdf/Dissertation_Jens_Bender.pdf)  
752 [siegen.de/opus/volltexte/2015/965/pdf/Dissertation\\_Jens\\_Bender.pdf](http://dokumentix.uw.uni-siegen.de/opus/volltexte/2015/965/pdf/Dissertation_Jens_Bender.pdf), 2015.
- 753 Bevacqua, E., De Michele, C., Manning, C., Couasnon, A., Ribeiro, A. F. S., Ramos, A. M., et al.: Guidelines for studying  
754 diverse types of compound weather and climate events, *Earth's Future*, 9:e2021EF002340,  
755 <https://doi.org/10.1029/2021EF002340>, 2021.
- 756 Bevacqua, E., Maraun, D., Hobæk Haff, I., Widmann, M., and Vrac, M.: Multivariate statistical modelling of compound events  
757 via pair-copula constructions: analysis of floods in Ravenna (Italy), *Hydrol. Earth Syst. Sci.*, 21, 2701–2723.  
758 <https://doi.org/10.5194/hess-21-2701-2017>, 2017.
- 759 Bevacqua, E., Suarez-Gutierrez, L., Jézéquel, A., Lehner, F., Vrac, M., Yiou, P., and Zscheischler J.: Advancing research on  
760 compound weather and climate events via large ensemble model simulations, *Nat. Commun.*, 14, 2145,  
761 <https://doi.org/10.1038/s41467-023-37847-5>, 2023.
- 762 Birant, D., and Kut, A.: ST-DBSCAN: An algorithm for clustering spatial-temporal data. *Data Know. Eng.*, 60, 208–221,  
763 <https://doi.org/10.1016/j.datak.2006.01.013>, 2007.
- 764 Blauhut, V., Stoelzle, M., Ahopelto, L., Brunner, M. I., Teutschbein, C., Wendt, D. E., Akstinas, V., Bakke, S. J., Barker, L.  
765 J., Bartošová, L., Briede, A., Cammalleri, C., Kalin, K. C., De Stefano, L., Fendeková, M., Finger, D. C., Huysmans, M.,  
766 Ivanov, M., Jaagus, J., Jakubínský, J., Krakovska, S., Laaha, G., Lakatos, M., Manevski, K., Neumann Andersen, M.,  
767 Nikolova, N., Osuch, M., van Oel, P., Radeva, K., Romanowicz, R. J., Toth, E., Trnka, M., Urošev, M., Urquijo Reguera,  
768 J., Sauquet, E., Stevkov, A., Tallaksen, L. M., Trofimova, I., Van Loon, A. F., van Vliet, M. T. H., Vidal, J.-P., Wanders,  
769 N., Werner, M., Willems, P., and Živković, N.: Lessons from the 2018–2019 European droughts: a collective need for  
770 unifying drought risk management, *Nat. Hazards Earth Syst. Sci.*, 22, 2201–2217, [https://doi.org/10.5194/nhess-22-2201-](https://doi.org/10.5194/nhess-22-2201-2022)  
771 [2022](https://doi.org/10.5194/nhess-22-2201-2022), 2022.
- 772 Brakkee, E., van Huijgevoort, M. H. J., and Bartholomeus, R. P.: Improved understanding of regional groundwater drought  
773 development through time series modelling: the 2018–2019 drought in the Netherlands, *Hyd. Earth Sys. Sci.*, 26, 551–569.  
774 <https://doi.org/10.5194/hess-26-551-2022>, 2022.
- 775 Brauns, B., Cuba, D., Bloomfield, J. P., Hannah, D. M., Jackson, C., Marchant, B. P., et al.: The Groundwater Drought  
776 Initiative (GDI): Analysing and understanding groundwater drought across Europe, *Proc. Int. Assoc. Hydrol. Sci.*, 383,  
777 297–305. <https://doi.org/10.5194/piahs-383-297-2020>, 2020.

- 778 Brun, P., Psomas, A., Ginzler, C., Thuiller, W., Zappa, M., and Zimmermann, N. E.: Large-scale early-wilting response of  
779 Central European forests to the 2018 extreme drought, *Glob. Change Biol.*, 26, 7021-7035, 2020.
- 780 Büchner, M., and Reyer, C.: ISIMIP3a atmospheric composition input data (v1.2). ISIMIP Repository.  
781 <https://doi.org/10.48364/ISIMIP.664235.2>, 2022
- 782 Bundesministerium für Ernährung und Landwirtschaft (BMEL): Ergebnisse der Waldzustandserhebung 2020,  
783 [https://www.bmel.de/SharedDocs/Downloads/DE/\\_Wald/ergebnisse-waldzustandserhebung-2020.html](https://www.bmel.de/SharedDocs/Downloads/DE/_Wald/ergebnisse-waldzustandserhebung-2020.html), 2021, (Accessed  
784 19 October 2024)
- 785 Buras, A., Rammig, A., and Zang, C. S.: Quantifying impacts of the 2018 drought on European ecosystems in comparison to  
786 2003, *Biogeosciences*, 17, 1655-1672, 2020.
- 787 Caldeira, M.C., Lecomte, X., David, T.S., Pinto, J.G., Bugalho, M.N., and Werner, C.: Synergy of extreme drought and plant  
788 invasion reduce ecosystem functioning and resilience. *Sci. Reports*, 5, 15110 <https://doi.org/10.1038/srep15110>, 2015
- 789 Carnicer, J., Alegria, A., Giannakopoulos, C. et al.: Global warming is shifting the relationships between fire weather and  
790 realized fire-induced CO<sub>2</sub> emissions in Europe, *Sci. Rep.*, 12, 10365, <https://doi.org/10.1038/s41598-022-14480-8>, 2022
- 791 Cerlini, P. B., Silvestri, L., Meniconi, S., and Brunone, B.: Simulation of the Water Table Elevation in Shallow Unconfined  
792 Aquifers by means of the ERA5 Soil Moisture Dataset: The Umbria Region Case Study, *Earth Inter.*, 25, 15–32.  
793 <https://doi.org/10.1175/EI-D-20-0011.1>, 2021.
- 794 Conradt, T., Engelhardt, H., Menz, C. et al.: Cross-sectoral impacts of the 2018–2019 Central European drought and climate  
795 resilience in the German part of the Elbe River basin, *Reg. Environ. Change*, 23, [https://doi.org/10.1007/s10113-023-](https://doi.org/10.1007/s10113-023-02032-3)  
796 02032-3, 2023.
- 797 Cornes, R.C., van der Schrier, G., van den Besselaar, E.J.M., and Jones, P.D.: An Ensemble Version of the E-OBS Temperature  
798 and Precipitation Data Sets, *J. Geophys. Res. Atmospheres* 123, 9391–9409. <https://doi.org/10.1029/2017JD028200>, 2018.
- 799 Cooley, D., and Thibaud, E.: Decompositions of dependence for high-dimensional extremes, *Biometrika*, 106, 587-604, 2019.
- 800 Cucchi, M., Weedon, G. P., Amici, A., Bellouin, N., Lange, S., Müller Schmied, H., Hersbach, H., and Buontempo, C.:  
801 WFDE5: bias-adjusted ERA5 reanalysis data for impact studies, *Earth Sys. Sci. Data*, 12, 2097–2120.  
802 <https://doi.org/10.5194/essd-12-2097-2020>, 2020.
- 803 Di Capua, G., Sparrow, S., Kornhuber, K., Rousi, E., Osprey, S., Wallom, D., van den Hurk, B. and Coumou, D.: Drivers  
804 behind the summer 2010 wave train leading to Russian heatwave and Pakistan flooding, *npj Clim. Atmos. Sci.*, 4, 55,  
805 <https://doi.org/10.1038/s41612-021-00211-9>, 2021.
- 806 D’Agostino, V.: Drought in Europe summer 2018: Crisis management in an orderly chaos, *Farm-Europe*, [https://www.farm-](https://www.farm-europe.eu/blog-en/drought-in-europe-summer-2018-crisis-management-in-an-orderly-chaos/)  
807 [europe.eu/blog-en/drought-in-europe-summer-2018-crisis-management-in-an-orderly-chaos/](https://www.farm-europe.eu/blog-en/drought-in-europe-summer-2018-crisis-management-in-an-orderly-chaos/), 2018, (Accessed 19 October  
808 2024).
- 809 D’Amato, J., Hantz, D., Guerin, A., Jaboyedoff, M., Baillet, L., and Mariscal, A.: Influence of meteorological factors on  
810 rockfall occurrence in a middle mountain limestone cliff, *Nat. Hazards Earth Syst. Sci.*, 16, 719–735,  
811 <https://doi.org/10.5194/nhess-16-719-2016>, 2016.

- 812 Dacre, H.F., Hawcroft, M.K., Stringer, M.A. and Hodges, K.I.: An extratropical cyclone database: A tool for illustrating  
813 cyclone structure and evolution characteristics, *Bull. Amer. Meteorol. Soc.*, 93, 1497-1502, [https://doi.org/10.1175/BAMS-](https://doi.org/10.1175/BAMS-D-11-00164.1)  
814 [D-11-00164.1](https://doi.org/10.1175/BAMS-D-11-00164.1), 2012.
- 815 de Brito, M., Kuhlicke, C. and Marx, A.: Near-real-time drought impact assessment: a text mining approach on the 2018/19  
816 drought in Germany, *Environ. Res. Lett.*, 15, 1040a9, 2020.
- 817 Deutscher Wetterdienst, 2018: Monatlicher Klimastatus Deutschland August 2018. DWD, Geschäftsbereich Klima und  
818 Umwelt, Offenbach, 29 Seiten,  
819 [www.dwd.de/DE/derdwd/bibliothek/fachpublikationen/selbstverlag/selbstverlag\\_node.html](http://www.dwd.de/DE/derdwd/bibliothek/fachpublikationen/selbstverlag/selbstverlag_node.html) (Accessed: 19th October  
820 2024).
- 821 Drouard, M., Kornhuber, K., and Woollings, T.: Disentangling dynamic contributions to summer 2018 anomalous weather  
822 over Europe, *Geophys. Res. Lett.*, 46, 12537–12546, 2019.
- 823 Dyrddal, A.V., Stordal, F., Lussana, C.: Evaluation of summer precipitation from EURO-CORDEX fine-scale RCM  
824 simulations over Norway, *Int. J. Clim.*, 38, 1661-1677, <https://doi.org/10.1002/joc.5287>, 2017
- 825 Eisenstein, L., Schulz, B., Qadir, G. A., Pinto, J. G. and Knippertz, P.: Identification of high-wind features within extratropical  
826 cyclones using a probabilistic random forest – Part 1: Method and case studies, *Weather Clim. Dynam.*, 3, 1157–1182,  
827 <https://doi.org/10.5194/wcd-3-1157-2022>, 2022.
- 828 Ellsäßer, F. and Xoplaki, E.: Cropdata – spatial yield productivity data base for the ten most cultivated crops in Germany from  
829 1989 to 2020 - version 1.0. <http://dx.doi.org/10.22029/jlupub-7177>, 2022a.
- 830 Ellsäßer, F. and Xoplaki, E.: Cropdata – yield anomaly catalogue for the ten most cultivated crops in Germany from 1989 to  
831 2020 - version 1.0. <http://dx.doi.org/10.22029/jlupub-7176>, 2022b.
- 832 Ellsäßer, F. and Xoplaki, E.: Cropdata – supplementary data (for spatial yield productivity data base for the ten most cultivated  
833 crops in Germany from 1989 to 2020) - version 1.0. <http://dx.doi.org/10.22029/jlupub-7203>, 2022c.
- 834 Ester, M., Kriegel, H.P. Sander, J., Xu, X., Simoudis, E., Han, J., and Fayyad, U.M. (eds.): A density-based algorithm for  
835 discovering clusters in large spatial databases with noise. *Proceedings of the Second International Conference on*  
836 *Knowledge Discovery and Data Mining (KDD-96)*. AAAI Press. pp. 226–231. CiteSeerX 10.1.1.121.9220. ISBN 1-57735-  
837 004-9, 1996
- 838 Feurdean, A., Vannière, B., Finsinger, W., Warren, D., Connor, S.C., Forrest, M., Liakka, J., et al.: Fire hazard modulation by  
839 long-term dynamics in land cover and dominant forest type in eastern and central Europe, *Biogeosciences*, 17, 1213–1230,  
840 2020.
- 841 Fischer, E. M., Seneviratne, S. I., Vidale, P. L., Lüthi, D., and Schär, C.: Soil moisture—atmosphere interactions during the  
842 2003 European summer heatwave, *J. Clim.*, 20: 5081–5099, 2007.
- 843 Fischer, E. M., and Schär, C.: Consistent geographical patterns of changes in high-impact European heatwaves, *Nat. Geosci.*,  
844 3, 398–403, <https://doi.org/10.1038/ngeo866>, 2010.

- 845 Fink, A. H., Brücher, T., Krüger, A., Leckebusch, G. C., Pinto, J. G. and Ulbrich, U.: The 2003 European summer heatwaves  
846 and drought –synoptic diagnosis and impacts, *Weather*, 59, 209–216, <https://doi.org/10.1256/wea.73.04>, 2004.
- 847 Fink, A. H., Brücher, T., Ermert, V., Krüger, A., and Pinto, J. G.: The European storm Kyrill in January 2007: synoptic  
848 evolution, meteorological impacts and some considerations with respect to climate change, *Nat. Hazards Earth Syst. Sci.*,  
849 9, 405–423, <https://doi.org/10.5194/nhess-9-405-2009>, 2009.
- 850 Frank, M.J.: On the simultaneous associativity of  $F(x,y)$  and  $x+y-F(x,y)$ , *Aequationes Mathematicae*, 19, 194-226, 1979.
- 851 Furusho-Percot, C., Goergen, K., Hartick, C., Kulkarni, K., Keune, J., and Kollet, S.: Pan-European groundwater to atmosphere  
852 terrestrial systems climatology from a physically consistent simulation, *Sci. Data.*, 6. [https://doi.org/10.1038/s41597-019-](https://doi.org/10.1038/s41597-019-0328-7)  
853 0328-7, 2019.
- 854 García-Herrera, R., Díaz, J., Trigo, R.M., Luterbacher, J., and Fischer, E. M.: A Review of the European Summer Heat Wave  
855 of 2003, *Crit. Rev. Env. Sci. Tech.*, 40, 267-306, <https://doi.org/10.1080/10643380802238137>, 2010.
- 856 Giorgi, F., Jones, C., and Arsar, G. R.: Addressing climate information needs at the regional level: the CORDEX framework,  
857 *WMO Bulletin*, 58, 175-183, 2009.
- 858 Hari, V., Rakovec, O., Markonis, Y., Hanel, M., and Kumar, R.: Increased future occurrences of the exceptional 2018–2019  
859 Central European drought under global warming, *Sci. Rep.*, 10, 1-10, 2020.
- 860 Hartick, C., Furusho-Percot, C., Goergen, K., & Kollet, S.: An interannual probabilistic assessment of subsurface water storage  
861 over Europe using a fully coupled terrestrial model, *Wat. Res. Res.*, 57, e2020WR027828, 2021.
- 862 Hersbach, H., and Coauthors: The ERA5 global reanalysis, *Q.J.R. Meteorol. Soc.*, 146, 1999-2049,  
863 <https://doi.org/10.1002/qj.3803>, 2020.
- 864 Hersbach, H., Bell, B., Berrisford, P., Biavati, G., Horányi, A., Muñoz Sabater, J., Nicolas, J., Peubey, C., Radu, R., Rozum,  
865 I., Schepers, D., Simmons, A., Soci, C., Dee, D., and Thépaut, J.-N.: ERA5 hourly data on single levels from 1940 to  
866 present. Copernicus Climate Change Service (C3S) Climate Data Store (CDS), <https://doi.org/10.24381/cds.adbb2d47>,  
867 2023.
- 868 Hlásny, T., Zimová, S., Merganičová, K., Štěpánek, P., Modlinger, R., and Turčáni, M: Devastating outbreak of bark beetles  
869 in the Czech Republic: Drivers, impacts, and management implications, *For. Ecol. Manage.*, 490,  
870 <https://doi.org/10.1016/j.foreco.2021.119075>, 2021.
- 871 Herzfeld, T., Heinke, J., Rolinski, S., and Müller, C.: Soil organic carbon dynamics from agricultural management practices  
872 under climate change, *Earth Sys. Dyn.*, 12, 1037–1055, <https://doi.org/10.5194/esd-12-1037-2021>, 2021.
- 873 IPCC: Impacts, Adaptation, and Vulnerability. Contribution of Working Group II to the Sixth Assessment Report of the  
874 Intergovernmental Panel on Climate Change [H.-O. Pörtner, D.C. Roberts, M. Tignor, E.S. Poloczanska, K. Mintenbeck,  
875 A. Alegría, M. Craig, S. Langsdorf, S. Löschke, V. Möller, A. Okem, B. Rama (eds.)]. Cambridge University Press.  
876 Cambridge University Press, Cambridge, UK and New York, NY, USA, 3056 pp., <https://doi.org/10.1017/9781009325844>,  
877 2022

- 878 Jane, R., Cadavid, L., Obeysekera, J., Wahl, T.: Multivariate statistical modelling of the drivers of compound flood events in  
879 south Florida. *Nat. Hazards Earth Syst. Sci.* 20, 2681–2699, <https://doi.org/10.5194/nhess-20-2681-2020>, 2020
- 880 Kaiser, D., Voynova, Y.G., and Brix, H.: Effects of the 2018 European heatwave and drought on coastal biogeochemistry in  
881 the German Bight, *Sci. Tot. Environ.*, 892, 164316, <https://doi.org/10.1016/j.scitotenv.2023.164316>, 2023
- 882 Kaspar, F., Friedrich, K., and Imbery, F.: Observed temperature trends in Germany: Current status and communication tools,  
883 *Meteorol. Z. (Contrib. Atm. Sci.)*, <https://doi.org/10.1127/metz/2023/1150>, 2023.
- 884 Kaspar, F., Müller-Westermeier, G., Penda, E., Mächel, H., Zimmermann, K., Kaiser-Weiss, A., and Deuschländer, T.:  
885 Monitoring of climate change in Germany – data, products and services of Germany’s National Climate Data Centre, *Adv.*  
886 *Sci. Res.*, 10, 99–106, <https://doi.org/10.5194/asr-10-99-2013>, 2013.
- 887 Kaspar, F., Zimmermann, K., and Polte-Rudolf, C.: An overview of the phenological observation network and the phenological  
888 database of Germany’s national meteorological service (Deutscher Wetterdienst), *Adv. Sci. Res.*, 11, 93–99, 2015.
- 889 Kautz, L.A., Martius, O., Pfahl, S., Pinto, J.G., Ramos, A.M., Sousa, P.M., and Woollings, T.: Atmospheric Blocking and  
890 Weather Extremes over the Euro-Atlantic Sector - A Review, *Weather Clim. Dynam.* 3, 305-336,  
891 <https://doi.org/10.5194/wcd-3-305-2022>, 2022
- 892 Kendall, M.G.: Rank correlation methods. 4 ed., 2. Impr. London: Griffin. ISBN 0852641990, 1975.
- 893 Kim, H.: Global Soil Wetness Project Phase 3 Atmospheric Boundary Conditions (Experiment 1) [Data set]. Data Integration  
894 and Analysis System (DIAS), <https://doi.org/10.20783/DIAS.501>, 2017.
- 895 Kohonen, T.: Essentials of the self-organizing map, *Neural Networks*, 37, 52–65,  
896 <https://doi.org/10.1016/j.neunet.2012.09.018>, 2013.
- 897 Kornhuber, K., Osprey, S., Coumou, D., Petri, S., Petoukhov, V., Rahmstorf, S. and Gray, L.: Extreme weather events in early  
898 Summer 2018 connected by a recurrent hemispheric wave pattern, *Environ. Res. Lett.*, 14, 054002,  
899 <https://doi.org/10.31223/osf.io/tq23m>, 2019.
- 900 Kornhuber, K., Coumou, D., Vogel, E., Lesk, C., Donges, J. F., Lehmann, J. and Horton, R. M.: Amplified Rossby waves  
901 enhance risk of concurrent heatwaves in major breadbasket regions, *Nat. Clim. Chang.*, 10, 48–53,  
902 <https://doi.org/10.1038/s41558-019-0637-z>, 2020.
- 903 Lange, S., Mengel, M., Treu, S., and Büchner, M.: ISIMIP3a atmospheric climate input data (v1.0), ISIMIP Repository,  
904 <https://doi.org/10.48364/ISIMIP.982724>, 2022.
- 905 Leonard, M., Westra, S., Phatak, A., Lambert, M., van den Hurk, B., McInnes, K., Risbey, J., Schuster, S., Jakob, D., and  
906 Stafford-Smith, M.: A compound event framework for understanding extreme impacts, *WIREs. Clim. Change*, 5, 113–  
907 128, <https://doi.org/10.1002/wcc.252>, 2014.
- 908 Leuschner, C.: Drought response of European beech (*Fagus sylvatica* L.) – a review, *Persp. Plant Ecol., Evol. and Syst.*, 47,  
909 125576, <https://doi.org/10.1016/j.ppees.2020.125576>, 2020.

- 910 Lidskog, R., Johansson, J., and Sjödin, D.: Wildfires, responsibility and trust: public understanding of Sweden's largest wildfire,  
911 *Scand. J. For. Res.*, 34, 319-328, 2019.
- 912 Liu, Xuebang, et al.: Similarities and differences in the mechanisms causing the European summer heatwaves in 2003, 2010,  
913 and 2018, *Earth's Future*, 7, e2019EF001386, <https://doi.org/10.1029/2019EF001386>, 2020.
- 914 Lorenz, R., Jaeger, E. B., and Seneviratne, S. I.: Persistence of heat waves and its link to soil moisture memory, *Geophys. Res.*  
915 *Lett.*, 37, L09703, 2010.
- 916 Lutz, F., Herzfeld, T., Heinke, J., Rolinski, S., Schaphoff, S., von Bloh, W., Stoorvogel, J. J. J., and Müller, C.: Simulating the  
917 effect of tillage practices with the global ecosystem model LPJmL (version 5.0-tillage), *Geosci. Mod. Develop.*, 12, 2419–  
918 2440, <https://doi.org/10.5194/gmd-12-2419-2019>, 2019.
- 919 Luterbacher, J., Dietrich, D., Xoplaki, E., Grosjean, M. and Wanner, H.: European seasonal and annual temperature variability,  
920 trends and extremes since 1500, *Science*, 303: 1499–1503, 2004.
- 921 Manning, C., Widmann, M., Bevacqua, E., Van Loon, A. F., Maraun, D., and Vrac, M.: Soil moisture drought in Europe: a  
922 compound event of precipitation and potential evapotranspiration on multiple time scales, *J. Hydrometeorol.*, 19, 1255–  
923 1271, <https://doi.org/10.1175/JHM-D-18-0017.1>, 2018.
- 924 Manning, C., Widmann, M., Maraun, D., Van Loon, A. F., and Bevacqua, E.: Large spread in the representation of compound  
925 long-duration dry and hot spells over Europe in CMIP5, *Weather Clim. Dynam.*, 4, 309–329, <https://doi.org/10.5194/wcd-4-309-2023>, 2023.
- 927 Manning, C., Kendon, E.J., Fowler, H.J., Catto, J.F., Chan, S.C., and Sansom, P.G.: Compound wind and rainfall extremes:  
928 Drivers and future changes over the UK and Ireland, *Wea. and Clim. Extremes*, 44, 100673,  
929 <https://doi.org/10.1016/j.wace.2024.100673>, 2024
- 930 McKee, T. B., Doesken, N. J., and Kleist, J.: The relationship of drought frequency and duration to time scales, Eighth  
931 Conference on Appl. Climatol., 179–184, 1993.
- 932 Martius, O.; Pfahl, S. and Chevalier, C.: A global quantification of compound precipitation and wind extremes, *Geophys. Res.*  
933 *Lett.*, 43, 7709–7717, <https://doi.org/10.1002/2016GL070017>, 2016.
- 934 Matzarakis, A., Laschewski, G., and Muthers, S.: The Heat Health Warning System in Germany—Application and Warnings  
935 for 2005 to 2019, *Atmosphere*, 11, 170, <https://doi.org/10.3390/atmos11020170>, 2020.
- 936 Messmer, M. and Simmonds, I.: Global analysis of cyclone-induced compound precipitation and wind extreme events, *Weath.*  
937 *Clim. Extremes*, 32, 100324, 2021.
- 938 Milanovic, S., Markovic, N., Pamucar, D., Gigovic, L., Kostic, P. and Milanovic, S.D.: Forest Fire Probability Mapping in  
939 Eastern Serbia: Logistic Regression versus Random Forest Method, *Forests*. 12: 5, <https://doi.org/10.3390/f12010005>,  
940 2021.
- 941 Miralles, D.G., Gentile, P., Seneviratne, S.I. and Teuling, A.J.: Land–atmospheric feedbacks during droughts and heatwaves:  
942 state of the science and current challenges, *Ann. N.Y. Acad. Sci.*, 1436: 19-35, <https://doi.org/10.1111/nyas.13912>, 2019

- 943 Mohr, S., Wandel, J., Lenggenhager, S., and Martius, O.: Relationship between atmospheric blocking and warm season  
 944 thunderstorms over western and central Europe, *Q. J. Roy. Meteor. Soc.*, 145, 3040–3056, <https://doi.org/10.1002/qj.3603>,  
 945 2019.
- 946 Mohr, S., Wilhelm, J., Wandel, J., Kunz, M., Portmann, R., Punge, H. J., Schmidberger, M., Quinting, J. F., and Grams, C.:  
 947 The role of large-scale dynamics in an exceptional sequence of severe thunderstorms in Europe May/June 2018, *Weather*  
 948 *Clim. Dynam.*, 1, 325–348, <https://doi.org/10.5194/wcd-1-325-2020>, 2020.
- 949 Munich RE, Extreme storms, wildfires and droughts cause heavy nat cat losses in 2018. 08/01/2019 Media Information,  
 950 available at: [https://www.munichre.com/en/company/media-relations/media-information-and-corporate-news/media-](https://www.munichre.com/en/company/media-relations/media-information-and-corporate-news/media-information/2019/2019-01-08-media-information.html)  
 951 [information/2019/2019-01-08-media-information.html](https://www.munichre.com/en/company/media-relations/media-information-and-corporate-news/media-information/2019/2019-01-08-media-information.html), 2019.
- 952 Naturgefahrenreport 2019, Die Schaden-Chronik der deutschen Versicherer, Gesamtverband der Deutschen  
 953 Versicherungswirtschaft, 56 pages e. V.,  
 954 [https://www.gdv.de/resource/blob/51710/e5eaa53a9ec21fb9241120c1d1850483/naturgefahrenreport-2019-schaden-](https://www.gdv.de/resource/blob/51710/e5eaa53a9ec21fb9241120c1d1850483/naturgefahrenreport-2019-schaden-chronik-data.pdf)  
 955 [chronik-data.pdf](https://www.gdv.de/resource/blob/51710/e5eaa53a9ec21fb9241120c1d1850483/naturgefahrenreport-2019-schaden-chronik-data.pdf) (Accessed 19 October 2024).
- 956 Nissen, K. M., Rupp, S., Kreuzer, T. M., Guse, B., Damm, B., and Ulbrich, U.: Quantification of meteorological conditions  
 957 for rockfall triggers in Germany, *Nat. Hazards Earth Syst. Sci.*, 22, 2117–2130, [https://doi.org/10.5194/nhess-22-2117-](https://doi.org/10.5194/nhess-22-2117-2022)  
 958 2022, 2022.
- 959 Nogueira, M.: Inter-comparison of ERA-5, ERA-Interim and GPCP rainfall over the last 40 years: process-based analysis of  
 960 systematic and random differences, *J. Hydrol.*, 583, 124632, <https://doi.org/10.1016/j.jhydrol.2020.124632>, 2020.
- 961 OECD.: Managing Climate Risks, Facing up to Losses and Damages, OECD Publishing, Paris,  
 962 <https://doi.org/10.1787/55ea1cc9-en>, 2021.
- 963 Öhrn, P., Berlin, M., Elfstrand, M., Krokene, P., and Jönsson, A. M.: Seasonal variation in Norway spruce response to  
 964 inoculation with bark beetle-associated bluestain fungi one year after a severe drought, *For. Ecol. Manage.*, 496, 119443,  
 965 2021.
- 966 Olonscheck, D., Suarez-Gutierrez, L., Milinski, S., et al.: The new Max Planck Institute Grand Ensemble with CMIP6 forcing  
 967 and high-frequency model output, *Authorea*, <https://doi.org/10.22541/essoar.168319746.64037439/v1>, May 4, 2023.
- 968 Orth, R., and Seneviratne, S. I.: Analysis of soil moisture memory from observations in Europe, *J. Geophys. Res.*, 117, D15115,  
 969 <https://doi.org/10.1029/2011JD017366>, 2012.
- 970 Pinto, J. G., Spanghel, T., Ulbrich, U., and Speth, P.: Sensitivities of a cyclone detection and tracking algorithm: individual  
 971 tracks and climatology, *Met. Zeitschrift*, 14, 823 – 838, <https://doi.org/10.1127/0941-2948/2005/0068>, 2005.
- 972 Pinto, J. G., Zacharias, S., Fink, A.H., Leckebusch, G.C, and Ulbrich, U.: Factors contributing to the development of extreme  
 973 North Atlantic cyclones and their relationship with the NAO, *Clim. Dynam.*, 32, 711–737, [https://doi.org/10.1007/s00382-](https://doi.org/10.1007/s00382-008-0396-4)  
 974 008-0396-4, 2009.
- 975 Piper, D., Kunz, M., Ehmele, F., Mohr, S., Mühr, B., Kron, A., and Daniell, J.: Exceptional sequence of severe thunderstorms  
 976 and related flash floods in May and June 2016 in Germany – Part 1: Meteorological background, *Nat. Hazards Earth Syst.*  
 977 *Sci.*, 16, 2835–2850, <https://doi.org/10.5194/nhess-16-2835-2016>, 2016.

- 978 Piper, D. A., Kunz, M., Allen, J. T., and Mohr, S.: Investigation of the temporal variability of thunderstorms in Central and  
 979 Western Europe and the relation to large-scale flow and teleconnection patterns, *Q. J. Roy. Meteor. Soc.*, 145, 3644–3666,  
 980 <https://doi.org/10.1002/qj.3647>, 2019.
- 981 Rauthe, M., Steiner, H., Riediger, U., Mazurkiewicz, A., and Gratzki, A.: A Central European precipitation climatology – Part  
 982 I: Generation and validation of a high-resolution gridded daily data set (HYRAS), *Meteorol. Z.*, 22, 235–256,  
 983 <https://doi.org/10.1127/0941-2948/2013/0436>, 2013.
- 984 Raymond, C., Horton, R.M., Zscheischler, J., Martius, O., AghaKouchak, A., Balch, J., Bowen, S. G., Camargo, S. J., Hess,  
 985 J., Kornhuber, K., Oppenheimer, M., Ruane, A. C., Wahl, T., and White, K.: Understanding and managing connected  
 986 extreme events, *Nat. Clim. Chang.*, 10, 611–621, <https://doi.org/10.1038/s41558-020-0790-4>, 2020.
- 987 Resnick, S. I.: *Heavy-tail phenomena: probabilistic and statistical modelling*, Springer Science & Business Media, 2007.
- 988 Riahi, K., van Vuuren, D.P., et al.: The Shared Socioeconomic Pathways and their energy, land use, and greenhouse gas  
 989 emissions implications: An overview, *Glob. Environ. Change*, 42, 153–168,  
 990 <https://doi.org/10.1016/j.gloenvcha.2016.05.009>, 2017.
- 991 Ridder, N., Pitman, A. J., Westra, S., Ukkola, A., Do, H., Bador, M., et al.: Global hotspots for the occurrence of compound  
 992 events, *Nat. Comm.*, 11, 5956, <https://doi.org/10.1038/s41467-020-19639-3>, 2020.
- 993 Ridder, N. N., Pitman, A. J., & Ukkola, A. M.: Do CMIP6 climate models simulate global or regional compound events  
 994 skillfully?, *Geophys. Res. Lett.* 48, e2020GL091152, <https://doi.org/10.1029/2020GL091152>, 2021.
- 995 Ridder, N.N., Ukkola, A.M., Pitman, A.J. et al.: Increased occurrence of high impact compound events under climate change,  
 996 *npj Clim. Atmos. Sci.*, 5, 3, <https://doi.org/10.1038/s41612-021-00224-4>, 2022.
- 997 Rösner, B. et al., The long heat wave and drought in Europe in 2018 [in “State of the Climate in 2018”], *Bull. Am. Meteorol.*  
 998 *Soc.*, 100, S222–S223, <https://doi.org/10.1175/2019BAMSStateoftheClimate.1>, 2019
- 999 Rupp S. and Damm, B.: A national rockfall dataset as a tool for analysing the spatial and temporal rockfall occurrence in  
 1000 Germany, *Earth Surf. Process. Landforms*, 45, 1528–1538, <https://doi.org/10.1002/esp.4827>, 2020.
- 1001 Rousi, E., Anagnostopoulou, C., Tolika, K. and Maheras, P.: Representing teleconnection patterns over Europe: A comparison  
 1002 of SOM and PCA methods, *Atmos. Res.*, 152, 123–137, <https://doi.org/10.1016/j.atmosres.2013.11.010>, 2015.
- 1003 Rousi, E., Kornhuber, K., Beobide-Arsuaga, G. et al.: Accelerated western European heatwave trends linked to more-persistent  
 1004 double jets over Eurasia, *Nat. Commun.*, 13, 3851, <https://doi.org/10.1038/s41467-022-31432-y>, 2022.
- 1005 Rousi, E., Fink, A. H., Andersen, L. S., Becker, F. N., Beobide-Arsuaga, G., Breil, M., Cozzi, G., Heinke, J., Jach, L.,  
 1006 Niermann, D., Petrovic, D., Richling, A., Riebold, J., Steidl, S., Suarez-Gutierrez, L., Tradowsky, J. S., Coumou, D.,  
 1007 Düsterhus, A., Ellsäßer, F., Fragkoulidis, G., Gliksman, D., Handorf, D., Hausteine, K., Kornhuber, K., Kunstmann, H.,  
 1008 Pinto, J. G., Warrach-Sagi, K., and Xoplaki, E.: The extremely hot and dry 2018 summer in central and northern Europe  
 1009 from a multi-faceted weather and climate perspective, *Nat. Hazards Earth Syst. Sci.*, 23, 1699–1718,  
 1010 <https://doi.org/10.5194/nhess-23-1699-2023>, 2023.



- 1011 Schaphoff, S., von Bloh, W., Rammig, A., Thonicke, K., Biemans, H., Forkel, M., Gerten, D., Heinke, J., Jägermeyr, J.,  
1012 Knauer, J., Langerwisch, F., Lucht, W., Müller, C., Rolinski, S., Waha, K., Knauer, J., von Bloh, W., Gerten, D., Jägermeyr,  
1013 J., and Waha, K.: LPJmL4 – a dynamic global vegetation model with managed land – Part 1: Model description, *Geosci.*  
1014 *Mod. Develop.* 11, 1343–1375, <https://doi.org/10.5194/gmd-11-1343-2018>, 2018.
- 1015 Schuldt, B., Knutzen, F., Delzon, S., Jansen, S., Müller-Haubold, H., Burrett, R., and Leuschner, C.: How adaptable is the  
1016 hydraulic system of European beech in the face of climate change-related precipitation reduction?, *New Phytol.*, 210, 443-  
1017 458, 2016.
- 1018 Schuldt, B., Buras, A., Arend, M., Vitasse, Y., Beierkuhnlein, C., Damm, A., and Kahmen, A.: A first assessment of the impact  
1019 of the extreme 2018 summer drought on Central European forests, *Basic Appl. Ecol.* 45, 86-103, 2020.
- 1020 Schulz, W., Diendorfer, G., Pedebay, S., and Poelman, D.R.: The European lightning location system EUCLID – Part 1:  
1021 Performance analysis and validation, *Nat. Hazards Earth Syst. Sci.*, 16, 595–605, [https://doi.org/10.5194/nhess-16-595-](https://doi.org/10.5194/nhess-16-595-2016)  
1022 2016, 2016.
- 1023 Seneviratne, S. I., et al.: Changes in climate extremes and their impacts on the natural physical environment. *Managing the*  
1024 *Risks of Extreme Events and Disasters to Advance Climate Change Adaptation*, C. B. Field et al., Eds., Cambridge  
1025 University Press, 109–230, 2012.
- 1026 Seneviratne, S.I., et al.: The Physical Science Basis. Contribution of Working Group I to the Sixth Assessment Report of the  
1027 Intergovernmental Panel on Climate Change [Masson-Delmotte, V., P. Zhai, A. Pirani, S.L. Connors, C. Péan, S. Berger,  
1028 N. Caud, Y. Chen, L. Goldfarb, M.I. Gomis, M. Huang, K. Leitzell, E. Lonnoy, J.B.R. Matthews, T.K. Maycock, T.  
1029 Waterfield, O. Yelekçi, R. Yu, and B. Zhou (eds.)]. Cambridge University Press, Cambridge, United Kingdom and New  
1030 York, NY, USA, pp. 1513–1766, <https://doi.org/10.1017/9781009157896.013>, 2021.
- 1031 Senf, C., and Seidl, R.: Persistent impacts of the 2018 drought on forest disturbance regimes in Europe, *Biogeosci.*, 18, 5223-  
1032 5230, 2021.
- 1033 Shyrokaya, A. et al.: Significant relationships between drought indicators and impacts for the 2018–2019 drought in  
1034 Germany, *Environ. Res. Lett.* 19 014037, 2024, DOI 10.1088/1748-9326/ad10d9
- 1035 Simpson, N.P., et al.: A framework for complex climate change risk assessment, *One Earth*, 4, 489–501,  
1036 <https://doi.org/10.1016/j.oneear.2021.03.005>, 2021.
- 1037 Statistische Ämter des Bundes und der Länder. Regionaldatenbank Deutschland,  
1038 <https://www.regionalstatistik.de/genesis/online/logon>, 2021.
- 1039 Song, Y.M., Wang, Z.F., Qi, L.L., and Huang, A.N.: Soil Moisture Memory and Its Effect on the Surface Water and Heat  
1040 Fluxes on Seasonal and Interannual Time Scales, *J. Geophys. Res. Atmos.*, 124, 10730–10741, 2019.
- 1041 Sousa, P. M., et al.: Distinct influences of large-scale circulation and regional feedbacks in two exceptional 2019 European  
1042 heatwaves, *Commun. Earth Environ.*, 1, 48, <https://doi.org/10.1038/s43247-020-00048-9>, 2020.
- 1043 Spensberger, C., Madonna, E., Boettcher, M., Grams, C. M., Papritz, L., Quinting, J. F., Röthlisberger, M., Sprenger, M. and  
1044 Zschenderlein, P.: Dynamics of concurrent and sequential Central European and Scandinavian heatwaves, *Q. J. R.*  
1045 *Meteorol. Soc.*, 146, 2998–3013, <https://doi.org/10.1002/QJ.3822>, 2020.

- 1046 Stefanon, M., D'Andrea, F. and Drobinski, P.: Heatwave classification over Europe and the Mediterranean region, *Environ.*  
1047 *Res. Lett.*, 7, 014023, <https://doi.org/10.1088/1748-9326/7/1/014023>, 2012.
- 1048 Szemkus S., and Friederichs P.: “Spatial patterns and indices for heat waves and droughts over Europe using a decomposition  
1049 of extremal dependency”. *Advances in Statistical Climatology, Meteorology and Oceanography* 10.1,  
1050 <https://doi.org/10.5194/ascmo-10-29-2024>, 2024.
- 1051 Taylor, K.E., Stouffer, R.J., and Meehl, G.A.: An Overview of CMIP5 and the experiment design, *Bull. Amer. Meteor. Soc.*,  
1052 93, 485-498, <https://doi.org/10.1175/BAMS-D-11-00094.1>, 2012.
- 1053 Tisdeman, E., and Menzel, L.: The development and persistence of soil moisture stress during drought across southwestern  
1054 Germany, *Hydrol. and Earth Sys. Sci.*, 25, 2009–2025, <https://doi.org/10.5194/hess-25-2009-2021>, 2021.
- 1055 Toreti, A., Belward, A., Perez-Dominguez, I., Naumann, G., Luterbacher, J., Cronie, O., Seguini, L., Manfron, G., Lopez-  
1056 Lozano, R., Baruth, B., Berg, M., Dentener, F., Ceglar, A., Chatzopoulos, T., and Zampieri, M.: The Exceptional 2018  
1057 European Water Seesaw Calls for Action on Adaptation, *Earth's Future* 7, 652–663,  
1058 <https://doi.org/10.1029/2019EF001170>, 2019a.
- 1059 Toreti, A., Cronie, O. & Zampieri, M. Concurrent climate extremes in the key wheat producing regions of the world, *Sci. Rep.*,  
1060 9, 5493, <https://doi.org/10.1038/s41598-019-41932-5>, 2019b.
- 1061 UNFCCC: Loss and Damage, online guide, United Nations Framework Convention on Climate Change, 46 pages,  
1062 [https://unfccc.int/sites/default/files/resource/loss\\_and\\_damage\\_online\\_guide.pdf](https://unfccc.int/sites/default/files/resource/loss_and_damage_online_guide.pdf), 2024 (Accessed 19 October 2024).
- 1063 van Delden, A.: The synoptic setting of thunderstorms in western Europe, *Atmos. Res.*, 56, 89–110,  
1064 [https://doi.org/10.1016/S0169-8095\(00\)00092-2](https://doi.org/10.1016/S0169-8095(00)00092-2), 2001.
- 1065 van der Wiel, K., Lenderink, G., and de Vries, H.: Physical storylines of future European drought events like 2018 based on  
1066 ensemble climate modelling, *Weath. Clim. Extremes*, 33, 100350, <https://doi.org/10.1016/j.wace.2021.100350>, 2021.
- 1067 Van Loon, A. F., and Van Lanen, H. A. J.: A process-based typology of hydrological drought. *Hydrol. Earth Syst. Sci.*, 16,  
1068 1915–1946, <https://doi.org/10.5194/hess-16-1915-2012>, 2012.
- 1069 Vautard, R., van Oldenborgh, G. J., Otto, F. E. L., Yiou, P., de Vries, H., van Meijgaard, E., Stepek, A., Soubeyroux, J.-M.,  
1070 Philip, S., Kew, S. F., Costella, C., Singh, R., and Tebaldi, C.: Human influence on European winter wind storms such as  
1071 those of January 2018, *Earth Syst. Dynam.*, 10, 271–286, <https://doi.org/10.5194/esd-10-271-2019>, 2019.
- 1072 Vicente-Serrano, S. M., Beguería, S., and López-Moreno, J.I.: A Multiscalar Drought Index Sensitive to Global Warming: The  
1073 Standardized Precipitation Evapotranspiration Index, *J. Climate*, 23, 1696-1718, <https://doi.org/10.1175/2009JCLI2909.1>,  
1074 2010.
- 1075 Vogel, M. M., Zscheischler, J., Wartenburger, R., Dee, D., and Seneviratne, S. I.: Concurrent 2018 hot extremes across  
1076 Northern Hemisphere due to human-induced climate change, *Earth's future*, 7, 692– 703,  
1077 <https://doi.org/10.1029/2019EF001189>, 2019.

1078 von Bloh, W., Schaphoff, S., Müller, C., Rolinski, S., Waha, K., and Zaehle, S.: Implementing the nitrogen cycle into the  
1079 dynamic global vegetation, hydrology, and crop growth model LPJmL (version 5.0), *Geosci. Model Develop.*, 11, 2789–  
1080 2812. <https://doi.org/10.5194/gmd-11-2789-2018>, 2018.

1081 Wetter3.de (n.d.): Die ganze Welt in Wetterkarte. Retrieved 5 December 2022, from [https://www.wetter3.de/index\\_dt.html](https://www.wetter3.de/index_dt.html)

1082 Wild, M.: Global dimming and brightening: A review, *J. Geophys. Res.*, 114, D00D16, <https://doi.org/10.1029/2008JD011470>,  
1083 2009.

1084 Wild, M.: Decadal changes in radiative fluxes at land and ocean surfaces and their relevance for global warming, *Wiley*  
1085 *Interdisc. Reviews: Climate Change*, 7, 91-107, 2016.

1086 Yang, J., and Tian, H.: ISIMIP3b N-deposition input data (v1.0). ISIMIP Repository. <https://doi.org/10.48364/ISIMIP.600567>,  
1087 2020.

1088 Zaitchik, B.F., Omumbo, J., Lowe, R., van Aalst, M., Anderson, L.O., Fischer, E., Norman, C., Robbins, J., Barciela, R.,  
1089 Trtanj, J., von Borries, R., and Luterbacher, J.: Planning for compound hazards during the COVID-19 pandemic: the role  
1090 of climate information systems. *Bull. Americ Meteorol. Soc.*, 103, E704-E709, 2022.

1091 Zampieri, M., Ceglar, A., Dentener, F., and Toreti, A.: Wheat yield loss attributable to heat waves, drought and water excess  
1092 at the global, national and subnational scales, *Environ. Res. Lett.* 12, 064008. <https://doi.org/10.1088/1748-9326/aa723b>,  
1093 2017.

1094 Zscheischler, J., and Fischer, E.M.: The record-breaking compound hot and dry 2018 growing season in Germany, *Weather*  
1095 *Clim. Extrem.*, 29, 100270. <https://doi.org/10.1016/j.wace.2020.100270>, 2020.

1096 Zscheischler, J., Martius, O., Westra, S., Bevacqua, E., Raymond, C., Horton, R. M., van den Hurk, B., AghaKouchak, A.,  
1097 Jézéquel, A., Mahecha, M. D., Maraun, D., Ramos, A. M., Ridder, N. N., Thiery, W. and Vignotto, E.: A typology of  
1098 compound weather and climate events, *Nat. Rev. Earth Environ.*, 1, 333–347, <https://doi.org/10.1038/s43017-020-0060-z>,  
1099 2020.

1100 Zscheischler, J. and Seneviratne, S.I.: Dependence of drivers affects risks associated with compound events, *Sci. Adv.* 3,  
1101 e1700263, 2017.